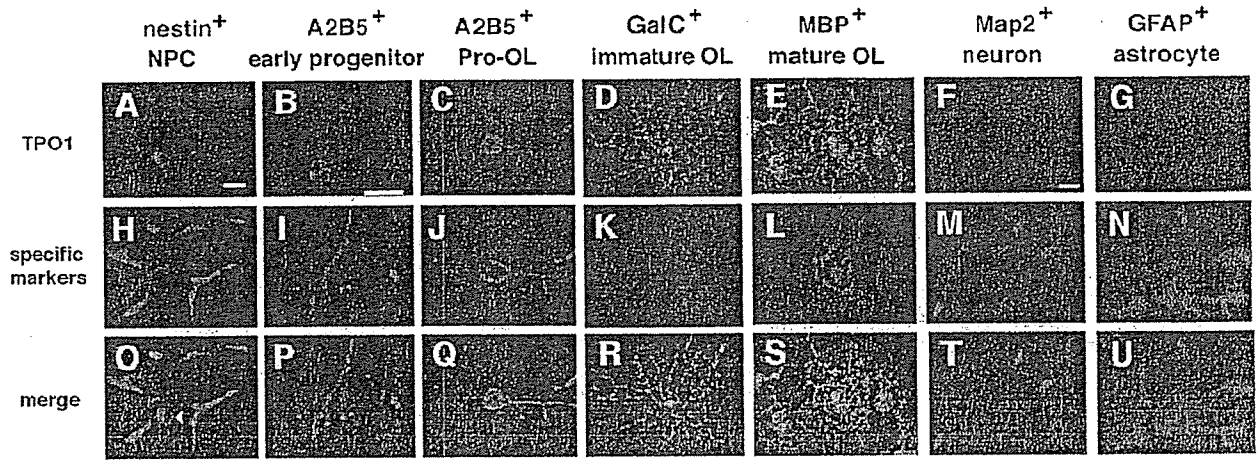

Fig. 5 – TPO1 is specifically expressed in OL lineage cells. TPO1 expression was evaluated in isolated CNS cells. Panels A, H and O: Neuroepithelial cells prepared from E14 mouse cortex. Panels B–E, I–L and P–S: OL lineage cells from P7 rat optic nerves. OPCs were cultured in differentiation medium for 6 hr (for early progenitors: B, I and P), 2 days (for Pro-OLs: C, J and Q), 4 days (for immature OLs: D, K and R) or 6 days (for mature OLs: E, L and S). Panels F, M and T: Primary cultured neurons were prepared from E14 mouse cortex. Panels G, N and U: Astrocytes from P1 mouse cortex. These cells were immunostained with anti-TPO1 (A–G) and anti-nestin (H), A2B5 (I and J), GalC (K), anti-MBP (L), anti-Map-2 (M) or anti-GFAP (N). Merged images are presented in panels O–U. Images A, H and O and F, G, M, N, T and U were obtained with a cooled CCD camera. Images B–E, I–L and P–S were obtained with a confocal laser microscope. Scale bars = 25 μm in A, F, G, H, M–O, T and U, and 20 μm in B–E, I–L and P–S.

Doolittle method (Kyte and Doolittle, 1982). In this work, we generated TPO1-specific antibodies and showed that TPO1 specifically distributes to the myelin membrane of Schwann cells and OLs and colocalizes with Fyn and GalC in cultured OLs. Our analyses suggested that TPO1 function may possibly be linked to the autophosphorylation of Fyn in the myelin membrane.

Phylogenetic analysis showed that TPO1 has diverged from AIGP1 and TMS2 (Fig. 1A). According to this evolutionary classification, the expression patterns of AIGP-family members in nervous systems have been divided into two groups: AIGP1 and TMS-2, which are expressed in neurons (Grossman et al., 2000; Aoki et al., 2002), and TPO1, which is expressed specifically in OLs and Schwann cells. Highly organized compact myelin is unique to vertebrates (Baumann and Pham-Dinh, 2001), thus *Drosophila melanogaster* lacks compact myelin and has only one AIGP family member, dTMS (Grossman et al., 2000), which is more similar to AIGP1 than TPO1 (Fig. 1A). These facts suggest that the evolutionary origins of compact myelin in vertebrates involved the emergence of the TPO1 gene and that TPO1 may play an important role in the formation and maintenance of compact myelin in vertebrates.

Trembler mice lack compact myelin in the PNS. The trembler phenotype is caused by an inherited mutation in the PMP22 gene (Suter et al., 1992; Suh et al., 1997; Sakai et al., 1999). The expression of the myelin membrane proteins P0, MBP and MAG is significantly reduced in the PNS, and the localization pattern of MAG is altered in Schwann cells of trembler mice (Vallat et al., 1999). In the present study, immunohistochemical analysis revealed that TPO1 expression is significantly reduced in the PNS myelin membrane of trembler-Ncnp mice, indicating that TPO1 is a myelin membrane protein. Furthermore we found that the localization pattern of TPO1 is altered in Schwann cells of the trembler mouse, and this altered pattern is similar to that of MAG in the trembler mouse (Vallat et al., 1999), suggesting a possible link between TPO1 and MAG in myelin formation and maintenance.

In the developing rodent brain, the proliferation of OL progenitors increases after birth. Myelin formation starts around P0 and largely occurs between P10 and P60 (Baumann and Pham-Dinh, 2001). The TPO1 gene expression is markedly upregulated from P10 to P20, an early phase of active myelination (Fig. 2). During this stage, immature OLs contact axons and transform into MBP(+) mature OLs. Previous studies have indicated that neuronal contact leads to the activation of PLP, MBP and MAG genes in OLs in vivo and in vitro (Macklin et al., 1986; Kidd et al., 1990; Matsuda et al., 1997). Together with its OL-specific localization, the expression profile of TPO1 in the developing brain suggests that the upregulation of gene expression in P10–20 mice may be triggered by neuron–OL interactions, which in turn may be involved in the induction of myelination. Thus, it is important to further elucidate the relationship between TPO1 and neuron–OL interaction.

Immunofluorescence analyses with organelle-specific markers showed that TPO1 localizes to Golgi in OL cell bodies. Previous experiments demonstrated that another family member, AIGP1, is similarly localized to the Golgi in neurons (Aoki et al., 2002). The basis of Golgi targeting of AIGP1 and TPO1 is not known, but AIGP family members likely use a common mechanism. The known AIGP family members do not have conventional Golgi targeting signals, suggesting that these proteins contain a novel Golgi targeting mechanism. On the other hand, TPO1 also localizes to OL processes and myelin-like sheets, and the myelin protein targeting may be achieved by palmitoylation (Schneider et al., 2005). The localization of TPO1 partially overlapped with that of Fyn,

which is also a palmitoylated protein (Shenoy-Scaria et al., 1993; Koegl et al., 1994; Wolven et al., 1997). Protein palmitoylation is a post-translational lipid modification that mediates interactions with cellular membranes (Han and Martinage, 1992; Koegl et al., 1994) and recruits multiple classes of signaling molecules to specialized membrane microdomains

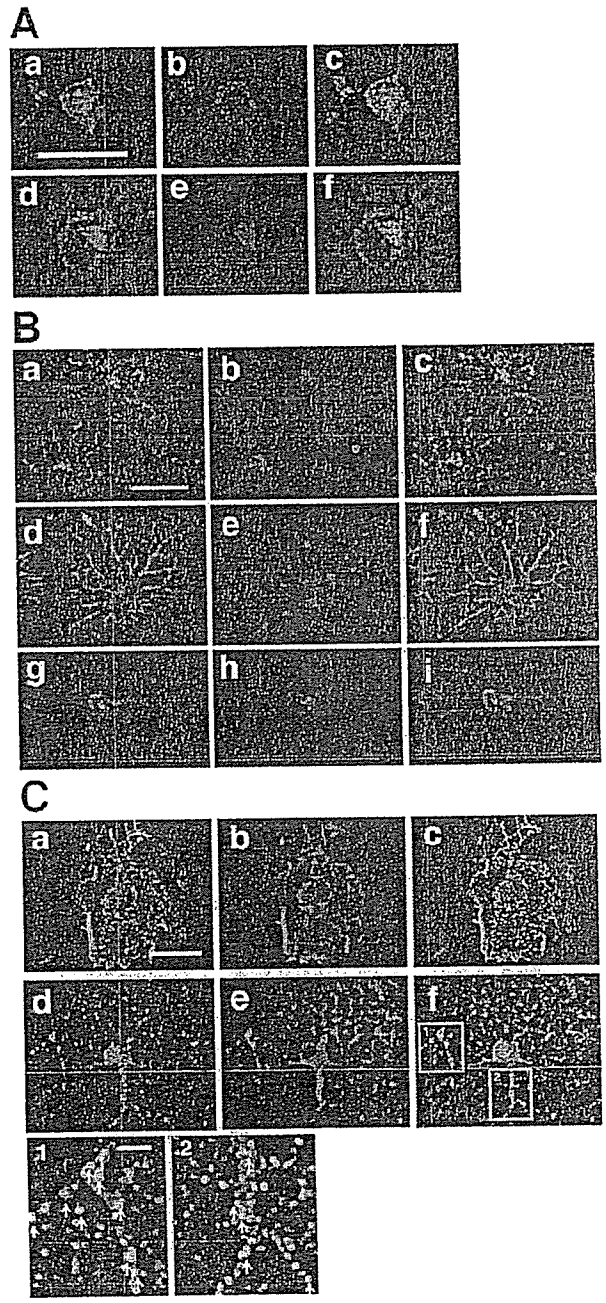

Fig. 6 – Subcellular localization of TPO1 in OLs. OPCs derived from rat optic nerve were cultured in differentiation medium for 6 days. Mature OLs with cell processes and myelin-like membrane sheets were double-stained with anti-TPO1 (A-a and A-d; B-a, B-d and B-g; and C-a, C-d and C-g) and the following organelle markers: anti-KDEL (endoplasmic reticulum; Ab), anti-GM130 (Golgi; Ae), anti-Lamp-1 (late endosomes and lysosomes; B-b), anti-Rab3a (secretory vesicles; B-e) and anti-EEA1 (early endosomes; B-h). Merged images are presented in A-c and A-f, and B-c, B-f and B-i. Images were obtained by confocal microscopy; scans through the cell bodies (A) and cell processes and myelin-like membrane sheets (B) are shown. Scale bars = 20 μm. (C) OLs with multiple cell processes (a–c) and myelin-like sheets (d–i) were double-stained with anti-TPO1 (a and d) and anti-GalC (b) or anti-Fyn (e). Merged images are presented in panels c and f. Images in region 1 and 2 of panel f were magnified and are presented in panels 1 and 2, respectively. Arrows in 1 and 2 indicate overlapping signals (yellow). Images were obtained by confocal microscopy. Scale bar (a) = 20 μm, Scale bar (1) = 5 μm.

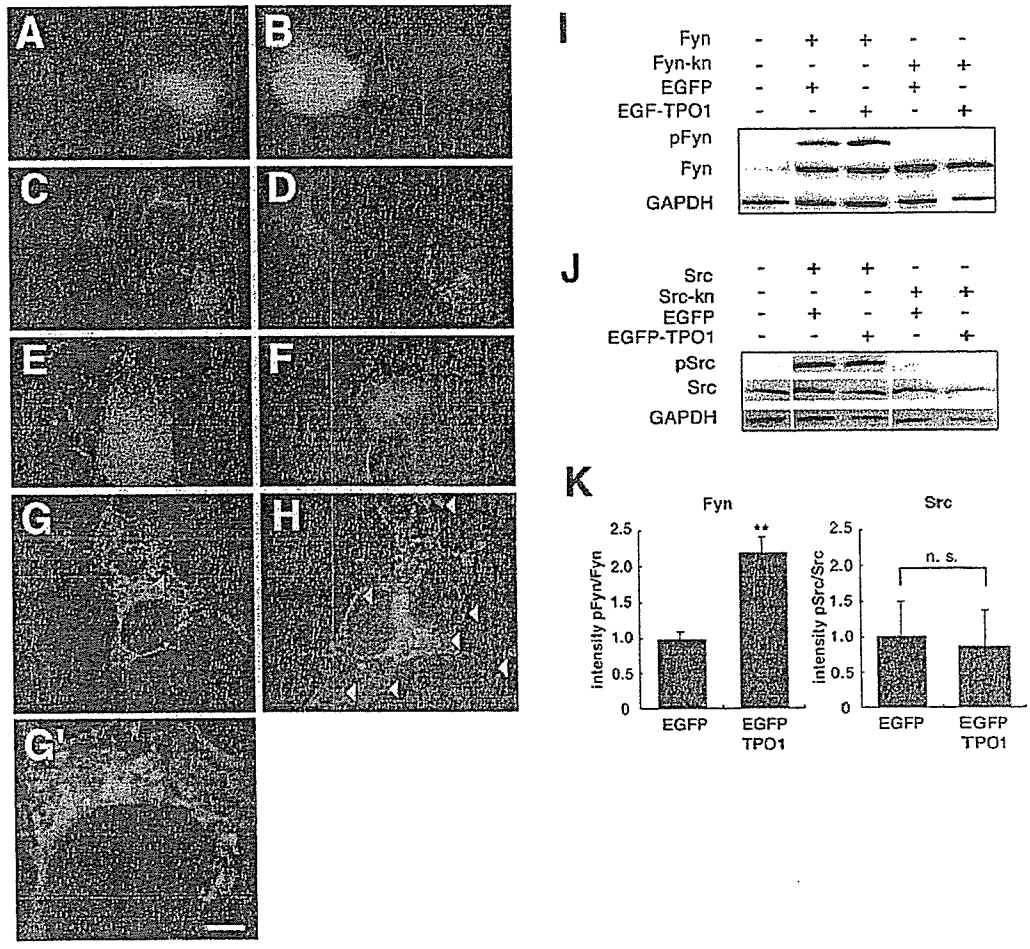

Fig. 7 – TPO1 promotes autophosphorylation of Fyn tyrosine kinase. (A–H) Immunocytochemical analyses of TPO1, Fyn and phosphorylated Fyn expression patterns. COS7 cells were cotransfected with pEGFP (A, B, E and F) or pEGFP-TPO1 (C, D, G and H) together with wild-type Fyn (E–G) or mock (A–D) expression vectors. After transient expression (for 24 hr), fixed cells were stained with anti-Fyn (A, C, E and G) or anti-phospho-Src family (B, D, F and H), and staining was visualized using red fluorescence. EGFP and EGFP-TPO1 are distributed in uniform (A, B, E and F) and in Golgi-like patterns (C, D, G and H), respectively. G′ is a magnified image derived from G. Arrows in G′ indicate overlapping signals (yellow). Images were obtained using a cooled CCD camera. Scale bar (A) = 10 μm, Scale bar (G′) = 5 μm. (I) Immunoblot analysis of phosphorylated Fyn. COS7 cells were cotransfected with pEGFP or pEGFP-TPO1 together with wild-type Fyn (wt) or kinase-negative (kn) Fyn expression vectors. Cell lysates were prepared and analyzed by immunoblotting with anti-phospho-Src family, anti-Fyn, or anti-GAPDH, as indicated. (J) Immunoblot analysis of phosphorylated Src. COS7 cells were cotransfected with pEGFP or pEGFP-TPO1 together with wild-type Src (wt) or kinase-negative (kn) Src expression vectors. Cell lysates were prepared and analyzed by immunoblotting with anti-phospho-Src family, anti-c-Src, or anti-GAPDH as indicated. (K) Relative Fyn and Src phosphorylation levels (phosphorylated Fyn or Src signal/total Fyn or Src signal/GAPDH signal) in pEGFP-TPO1-transfected cells and in pEGFP-transfected cells. Each bar represents the mean ± SEM ($n = 3$). $^{**}P < 0.01$.

(Simons and Ikonen, 1997; Verkade and Simons, 1997). Thus, TPO1 palmitoylation may be required for interactions with signal transduction molecules, including Fyn kinase.

In this study, we found that TPO1 promotes the autophosphorylation of Fyn kinase. Several lines of evidence suggest that Fyn is essential for myelination. Fyn-deficient mice exhibit abnormal myelination and loss of myelin content, and Fyn activity has been suggested to directly regulate MBP gene transcription (Umemori et al., 1999). In vitro experiments with cultured OLs have shown that Fyn is required for OL development and morphological differentiation (Osterhout et al., 1999; Sperber and McMorris, 2001; Klein et al., 2002; Colognato et al., 2004; Liang et al., 2004). Fyn is a non-receptor-type tyrosine kinase, coupling multiple cell surface membrane proteins to transduce extracellular signals. The cell surface membrane proteins, MAG, F3, NCAM120, FcRγ and integrin act as receptors coupled with Fyn in myelinating cells (Umemori et al., 1994; Kramer et al., 1999; Klein et al., 2002; Nakahara et al., 2003; Colognato et al., 2004; Liang et al., 2004), and these receptors have been proposed to mediate the cell–cell interactions/signaling necessary for myelin formation and maintenance. Although we demonstrated that cross linking of

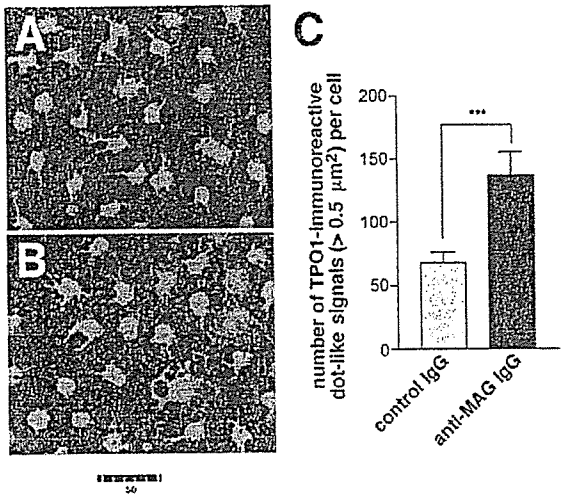

Fig. 8 – MAG cross-linking induces an increase in dot-like signals of TPO1 in immature OLs. (A, B) Immature OLs were incubated with control mouse IgG (A) or anti-mouse MAG IgG (B), followed by anti-mouse IgG. Cells were then immunostained with anti-TPO1. Images were obtained by confocal microscopy. Scale bar = 50 μm. (C) Quantification of the number of TPO1-immunoreactive dot-like signals (>0.5 μm²) per cell in the control IgG-treated or anti-MAG IgG-treated immature OLs. Each bar represents the mean ± SEM (n = 21 cells in each case). ***P < 0.001.

cell surface MAG altered the localization of TPO1 in OL-lineage cells (Fig. 8), it remains to be determined whether TPO1 is expressed at the cell surface and whether it directly interacts with Fyn and Fyn-associated receptors. TPO1 may function to regulate receptor-mediated signal that evoke Fyn kinase activation during myelination. Together with the proposed functions of AIGP1 in axonal damage and subsequent neuronal cell death (Aoki et al., 2002), a functional link between the AIGP family members may exist in neuron-OL/Schwann cell interactions. The elucidation of such a molecular link may be useful in clinical studies directed toward the prevention and treatment of myelin diseases.

4. Experimental procedures

4.1. *Antibodies*

The following monoclonal and polyclonal antibodies were used in this study: Monoclonal antibodies. RAN-2 (Bartlett et al., 1981), A2B5 (Eisenbarth et al., 1979), O4, anti-MAG, rat anti-MBP and anti-galactocerebroside (GalC) and anti-glyceraldehydes-3-phosphate dehydrogenase (GAPDH) (Chemicon International, Temecula, CA), Cy3-conjugated anti-glial fibrillary acidic protein (GFAP) (Sigma, St. Louis, MO), anti-microtubule-associated protein-2 (Map-2) (Leinco Technologies, St. Louis, MO), anti-KDEL and anti-lysosome-associated membrane glycoprotein-1 (Lamp-1) (Stressgen Biotechnologies, Victoria, BC), anti-GM130, anti-early endosome antigen1 (EEA1) and anti-Fyn (Transduction Laboratories, Lexington, KY), anti-Rab3a antibodies (Synaptic Systems, Göttingen, Germany). Polyclonal antibodies. Anti-c-Src (SRC 2) (Santa Cruz Biotechnology, Santa Cruz, CA) and anti-phospho-Src family (Tyr416) antibodies (Cell Signaling Technology, Beverly, MA). All Alexa Fluor fluorescein secondary antibody conjugates were purchased from Molecular Probes (Eugene, OR). Goat anti-mouse IgG for MAG cross-link was obtained from SouthernBiotech (Birmingham, AL).

4.2. *SYBR green-based real-time quantitative RT-PCR*

SYBR green-based real-time quantitative reverse transcription-polymerase chain reaction (RT-PCR) was performed as previously described (Wong et al., 2000; Aoki et al., 2002). Total RNA was isolated from whole brains of C57BL/6J mice at embryonic day 14 (E14), and postnatal days 1 (P1), 5, 10, 15, 20, 25 and 8 weeks. Total RNA (1 μg) was treated with DNase I and converted to cDNA using Superscript reverse transcriptase (Invitrogen, Carlsbad, CA) and random hexamer primers. Real-time RT-PCR was performed in a total reaction volume of 25 μl using an Applied Biosystems (Foster City, CA) 7700 Sequence Detection System. The following primer pairs were used: 5′-TGTTGGAGGCTTGGCTTTGA-3′ (nt 642–661; forward) and 5′-ACCAGAGAGATTAGCAGGCA-3′ (nt 733–752; reverse) for amplification of the TPO1 gene (GenBank accession no. AB029501); 5′-ATTCCTCTTCCTGCAGCACAG-3′ (nt 581–601; forward) and 5′-TGTTATCTTCCAGCAGGGCAC-3′ (nt 669–689; reverse) for amplification of the MOG gene (GenBank accession no. U64572); 5′-TGCTTCTGGTCCAGTGAATGG-3′ (nt 321–341; forward) and 5′-CGATGTAAGGTTGTCCCTTGG-3′ (nt 418–438; reverse) for amplification of the P0 gene (GenBank accession no. NM_008623); and 5′-AGAGACAACATTGGCATGGCT-3′ (nt 1282–1302; forward) and 5′-AATCCTGATCAAAAGCGCG-3′ (nt 1379–1498; reverse) for amplification of the β-actin gene (GenBank accession no. NM_007393) (Aoki et al., 2002). Control experiments (melting temperature analysis and agarose gel electrophoresis of PCR products) established that the signal for each amplicon was derived from cDNA and not from primer–dimers. The quantitative RT-PCR method (User Bulletin #2, Applied Biosystems) was modified to establish an expression level index for mRNA (Aoki et al., 2002), and all data were normalized to the SYBR green signal for β-actin amplicon.

4.3. *Antibody production*

Polyclonal antibodies against TPO1 (ABEP06 and ABEP05) were obtained by immunizing rabbits with the synthetic epitope peptide 06 (EP06) (VMKQVKDHIPSFE; aa 58–70 in mouse TPO1; GenBank accession no. AB029501) or epitope peptide 05 (EP05) (SDALQSRYGAPE; aa 339–350 in mouse TPO1). Rabbits were immunized with each peptide coupled to keyhole limpet hemocyanin in complete adjuvant four times at 2-week intervals. The resulting antisera were affinity-purified on EP05- or EP06-coupled peptide columns using a SulfoLink kit (Pierce, Rockford, IL) according to the manufacturer's protocol.

4.4. *Western blot analysis of TPO1*

Western Blotting was performed as described previously (Aoki et al., 2002), with minor modifications. Mouse cortical OLs cultured for 3 days were suspended in phosphate-buffered saline (PBS) containing complete protease inhibitor mixture (Roche, Lewes, East Sussex, UK) and lysed on ice using a Handy Sonic model UR-20P (power level 3–4; TOMY, Tokyo, Japan). To separate membrane and soluble fractions, the lysates were centrifuged at 12,000×g for 30 min at 4 °C. Protein concentration was determined using a protein assay kit (Bio-Rad, Hercules, CA), and equivalent amounts of soluble and membrane proteins from both fractions were resolved by electrophoresis on a 10–20% gradient sodium dodecyl sulfate-polyacrylamide gel (SDS-PAGE). The resolved proteins were then transferred to a PVDF membrane (Bio-Rad) using a semi-dry electroblotter (Bio-Rad). The membrane was blocked by incubation in 1% bovine serum albumin (BSA)/PBS containing 0.1% (v/v) Tween-20 for 1 hr at room temperature (RT). ABEP05 (1 μg/ml) or negative control normal rabbit IgG (1 μg/ml) was used as a primary antibody, and horseradish peroxidase (HRP)-conjugated

anti-rabbit IgG (H+L) (Dako, Carpinteria, CA) was used as secondary antibody. Immunoreactive bands were detected using the Super-signal Substrate System (Pierce) according to the manufacturer's instructions. The specificity of the TPO1 antibodies was evaluated using the following methods: (1) COS7 cells transfected with a C-terminal Myc-tagged mouse TPO1 expression construct were immunostained with an affinity-purified antibody against EP05 or 06 (ABEP05 or ABEP06). Staining showed Golgi-localized small puncta and completely overlapped that of anti-Myc (data not shown). No signal was observed in COS7 cells transfected with a mock construct (data not shown). (2) Affinity-purified ABEP05 and 06 antibodies were pre-incubated with 100-fold excess of EP05 and EP06 or with an unrelated peptide as a negative control. TPO1 staining was abolished by pre-absorption with the corresponding antigens (data not shown), and incubation with the negative control peptide had no effect on the staining pattern (data not shown). (3) As a negative control, cells or tissue sections were stained with rabbit IgG (Dako) at the same concentrations used in immunohistochemical experiments (Fig. 2Cd). No signal was observed. (4) Staining with anti-AIGP1 (a member of the AIGP protein family) or anti-TPO1 showed no myelin (Aoki et al., 2002) or neuronal staining (Figs. 3Ca, b and c), respectively, indicating no cross reactivity of the antibodies.

4.5. *Genotyping of trembler-Ncnp mice by genomic DNA PCR*

Genotyping of trembler-Ncnp mice was performed as described previously (Suh et al., 1997; Sakai et al., 1999). The two forward primers, 5′-TCAGGGACAGTACCAGAGCTCA-3′ and 5′-CCGTATT-TCTCGATCACACAC-3′, and the reverse primer, 5′-GAGCTAGT-TAGCTGCTGGACA-3′, were used for genotyping of wild-type, and trembler-Ncnp heterozygotes and homozygotes. The primer set can simultaneously amplify two different fragments to identify trembler-Ncnp and wild-type genotypes. PCR was performed using the GeneAmp PCR system 9700 (Applied Biosystems). Genomic DNA was pre-heated at 94 °C for 3 min, followed by 30 cycles of PCR (denaturation at 94 °C for 15 s, annealing at 57 °C for 2 min and polymerization at 72 °C for 2 min). After a final extension at 72 °C for 10 min, PCR products were analyzed on 2% agarose gels.

4.6. *Immunohistochemistry*

C57BL/6J mice were anesthetized and perfused with 4% paraformaldehyde (PFA). The brains were removed and post-fixed overnight, cryoprotected in 30% sucrose in PBS, and frozen in dry ice. Sections (20 μm) were cut with a Frigocut 2800 cryostat (Reichert-Jung, Wien, Austria), placed onto APS-coated glass slides, fixed with 4% PFA, washed three times with PBS, permeabilized with 0.1% (v/v) Triton X-100/PBS for 5 min and finally washed three times with PBS. Fixed sections were incubated for 30 min with 5% goat serum (Nichirei, Tokyo, Japan) in PBS. Sections were incubated overnight at 4 °C with diluted primary polyclonal and/or monoclonal antibody in 1% goat serum/PBS. These sections were incubated for 1 hr with diluted Alexa Fluor fluorescein-conjugated secondary antibody (Molecular Probes) and washed several times with PBS. Antibody dilutions were as follows: ABP05, 1 μg/ml; anti-Map2, 1:200; anti-GFAP, 1:200; O4, 1:50 and anti-MBP, 1:50. All secondary antibodies were used at a 1:200 dilution. Images of stained cells were obtained using a FluoView confocal microscope system (Olympus, Tokyo, Japan). For diaminobenzidine tetrahydrochloride (DAB) staining, paraffin sections (5 μm thick) of sciatic nerve and cerebellum from trembler-Ncnp and wild-type mice were prepared and stained with primary antibody. HRP-conjugated anti-rabbit antibody (Dako) was used as secondary antibody, and signals were visualized with DAB solution containing 0.3% H_2O_2 in PBS. Images were obtained with a CCD camera (HC-2500; Fujifilm, Kanagawa, Japan).

4.7. *Embryonic neuroepithelial cell culture*

Embryonic neuroepithelial cells were prepared from E14 mouse telencephalon as previously described (Nakashima et al., 1999). Cells were mechanically dissociated by trituration and plated on dishes (1.0×10^4 cells per dish; ϕ10 cm) coated with 15 μg/ml poly-L-ornithine (Sigma) and 1 μg/ml fibronectin (Asahi technoglass, Tokyo, Japan). Initially, plated cells were expanded for 4 days in B27-supplemented Neurobasal medium (Invitrogen) containing 10 ng/ml basic fibroblast growth factor (Peprotech, Rocky Hill, NJ) on dishes coated with poly-L-ornithine and fibronectin. Cells were then detached and replated on 4-well chamber slides (Nalgene Nunc International, Rochester, NY) at 5.0×10^4 cells per well for immunofluorescence staining.

4.8. *Immunopanning purification and cultivation of rat optic nerve oligodendrocyte precursor cells (OPCs)*

Rat optic nerve OPCs were prepared from optic nerves of P7 rats and purified by the immunopanning method (Barres et al., 1992) with minor modifications. Dissected optic nerves were mechanically dissociated and incubated for 75 min in a solution of 32 U/ml papain (Worthington, Freehold, NJ), 0.4 mg/ml L-cysteine (Sigma) and 0.004% DNase I (Sigma) in minimum essential medium (Invitrogen). Low ovomucoid trypsin inhibitor solution was added to stop the reaction. After centrifugation, the supernatant was removed and the cells suspended in high ovomucoid trypsin inhibitor solution. Cell aggregates were mechanically disrupted to single cells by pipetting, and then the cells were passed through a nylon mesh (20 μm pore size). After centrifugation, cells were suspended in L15/BSA medium (Invitrogen). The OPCs were purified by incubation of the cell suspension on a Ran2-coated dish for 20 min to remove type-1 astrocytes and microglia and then on an anti-GalC-coated dish for 30 min to remove mature OLs. Finally, cells were allowed to attach onto A2B5-coated dishes for 30 min. OPCs were detached from A2B5 dishes via trypsinization and replated on poly-D-lysine-coated flasks. OPCs were cultured in B-S medium: Dulbecco's modified Eagle' medium (DMEM) containing 10 μg/ml insulin, 5 ng/ml NT-3 (Peprotech), 100 μg/ml human transferrin, 100 μg/ml BSA, 60 ng/ml progesterone, 40 ng/ml sodium selenite, 63 μg/ml N-acetyl-cysteine, 16 μg/ml putrescine, 10 ng/ml D-biotin, 5 μM forskolin and penicillin–streptomycin–glutamine (Invitrogen) (other ingredients from Sigma). Human PDGF-AA (10 ng/ml, Peprotech) was added for proliferation of OPCs and then removed to induce differentiation of mature OLs.

4.9. *Immunocytochemistry*

Cultured cells were grown on poly-D-lysine-coated dishes for immunofluorescence staining. All incubations and washes were performed at RT. Cells were fixed with 4% PFA and then washed three times with PBS. Fixed cells were incubated for 30 min in blocking solution (1% BSA, 0.1% (v/v) Triton X-100, and 20% goat serum in 0.1 M PBS) and washed with PBS. Cells were incubated with diluted primary polyclonal and/or monoclonal antibody in the incubation buffer (1% BSA and 0.1% (v/v) Triton X-100 in PBS). Cells were then incubated for 30 min with diluted secondary antibody conjugated to Alexa Fluor fluorescein (Molecular Probes) and washed with PBS. Antibody concentrations and dilutions were as follows: ABEP05, 5 μg/ml; A2B5, 1:500; O4, 1:200; anti-GalC, 1:200; anti-MBP, 1:200; anti-Fyn, 1:200; and anti-phospho-Src family, 1:100. All secondary antibodies were diluted 1:200. Images were obtained using epifluorescence microscopy (Olympus IX70) or confocal microscopy (Olympus FluoView).

4.10. *Expression constructs*

To construct a TPO1-enhanced green fluorescent protein (EGFP) expression plasmid, a 1.4-kbp cDNA fragment of pCI-neo mouse

TPO1 (Aoki et al., 2002) was ligated between the *Xho*I and *Eco*RI sites of pEGFP-C1 (Invitrogen). Wild-type Fyn, kinase-negative Fyn (K299M), wild-type Src and kinase-negative Src (K299M) expression vectors (Takeuchi et al., 1993) were kindly provided by Dr. T. Yamamoto (Division of Oncology, Department of Cancer Biology, Institute of Medical Science University of Tokyo, Japan).

4.11. *Analyses of autophosphorylation of Fyn and Src*

COS7 cells were plated in 6-well dishes at a density of 4.0×10^4 cells/cm^2, cultured for 24 hr, and transfected with DNA using Lipofectamine (Invitrogen). After 6 hr, the medium was replaced with 0.1% fetal bovine serum/DMEM. At 18 hr post-transfection, the cells were washed twice with PBS and solubilized with RIPA buffer (20 mM Tris–HCl, pH 7.4, 150 mM NaCl, 1 mM EDTA, 1% (v/v) Nonidet P-40, 10% (v/v) glycerol, 0.1% SDS, 0.5% deoxycholate, 1 mM sodium orthovanadate and complete protease inhibitor mixture) for 20 min on ice. The lysate was centrifuged at 12,000×*g* for 30 min at 4 °C. Proteins were separated by SDS-PAGE and transferred electrophoretically to PVDF membranes. The membranes were blocked with 3% non-fat milk in Tris-buffered saline containing 0.1% (v/v) Tween-20 (T-TBS) for 1 hr at RT, incubated with primary antibodies in 3% BSA/T-TBS overnight at 4 °C, washed with T-TBS, incubated with HRP-conjugated secondary antibodies for 1 hr at RT, and washed with T-TBS. Antibodies were diluted as follows: anti-Fyn, 1:250; anti-c-Src, 1:50; anti-phospho-Src family, 1:1000; and anti-GAPDH, 1:300. Anti-mouse or anti-rabbit IgG (H+L) conjugated with HRP was used as secondary antibody. Immunoreactive bands were detected using the Supersignal Substrate System (Pierce) according to the manufacturer's instructions. The intensity of bands was quantified with FluorChem ver. 2.0 software (Alpha Innotech, San Leandro, CA).

4.12. *MAG cross-linking*

The MAG cross-linking experiment was performed as described (Marta et al., 2004) with minor modifications. Briefly, immature OLs were prepared by treatment with differentiation medium (B–S medium lacking PDGF-AA). The immature OLs were washed with DMEM and incubated for 15 min at 37 °C with monoclonal anti-MAG IgG (2.5 μg/ml) or control mouse IgG (2.5 μg/ml) diluted in B–S medium. The anti-MAG IgG or control IgG was washed out with DMEM, and the OLs were incubated with goat anti-mouse IgG (10 μg/ml) for 30 min at 37 °C and then fixed for immunocytochemistry.

Acknowledgments

We thank for Dr. Y. Tokumoto for technical advice and helpful suggestions. This work was supported by Grants-in-Aid for Scientific Research from the Ministry of Health, Labour and Welfare of Japan, Grants-in-Aid for Scientific Research from the Ministry of Education, Culture, Sports, science and Technology of Japan, a grant from the Organization for Pharmaceutical Safety and Research, a grant from Japan Science and Technology Cooperation, and new energy and industrial technology development organization (NEDO).

REFERENCES

Aoki, S., Su, Q., Li, H., Nishikawa, K., Ayukawa, K., Hara, Y., Namikawa, K., Kiryu-Seo, S., Kiyama, H., Wada, K., 2002. Identification of an axotomy-induced glycosylated protein, AIGP1, possibly involved in cell death triggered by endoplasmic reticulum-Golgi stress. J. Neurosci. 22, 10751–10760.

Barres, B.A., Hart, I.K., Coles, H.S., Burne, J.F., Voyvodic, J.T., Richardson, W.D., Raff, M.C., 1992. Cell death and control of cell survival in the oligodendrocyte lineage. Cell 70, 31–46.

Bartlett, P.F., Noble, M.D., Pruss, R.M., Raff, M.C., Rattray, S., Williams, C.A., 1981. Rat neural antigen-2 (RAN-2): a cell surface antigen on astrocytes, ependymal cells. Muller cells and lepto-meninges defined by a monoclonal antibody. Brain Res. 204, 339–351.

Baumann, N., Pham-Dinh, D., 2001. Biology of oligodendrocyte and myelin in the mammalian central nervous system. Physiol. Rev. 81, 871–927.

Chen, J.W., Murphy, T.L., Willingham, M.C., Pastan, I., August, J.T., 1985. Identification of two lysosomal membrane glycoproteins. J. Cell Biol. 101, 85–95.

Colognato, H., Ramachandrappa, S., Olsen, I.M., Ffrench-Constant, C., 2004. Integrins direct Src family kinases to regulate distinct phases of oligodendrocyte development. J. Cell Biol. 167, 365–375.

Eisenbarth, G.S., Walsh, F.S., Nirenberg, M., 1979. Monoclonal antibody to a plasma membrane antigen of neurons. Proc. Natl. Acad. Sci. U. S. A. 76, 4913–4917.

Fukuda, M., Kanno, E., Saegusa, C., Ogata, Y., Kuroda, T.S., 2002. Slp4-a/granuphilin-a regulates dense-core vesicle exocytosis in PC12 cells. J. Biol. Chem. 277, 39673–39678.

Grossman, T.R., Luque, J.M., Nelson, N., 2000. Identification of a ubiquitous family of membrane proteins and their expression in mouse brain. J. Exp. Biol. 203 (Pt. 3), 447–457.

Han, K.K., Martinage, A., 1992. Possible relationship between coding recognition amino acid sequence motif or residue(s) and post-translational chemical modification of proteins. Int. J. Biochem. 24, 1349–1363.

Hirayama, A., Oka, A., Ito, M., Tanaka, F., Okoshi, Y., Takashima, S., 2003. Myelin transcription factor 1 (MyT1) immunoreactivity in infants with periventricular leukomalacia. Brain Res. Dev. Brain Res. 140, 85–92.

Kidd, G.J., Hauer, P.E., Trapp, B.D., 1990. Axons modulate myelin protein messenger RNA levels during central nervous system myelination in vivo. J. Neurosci. Res. 26, 409–418.

Klein, C., Kramer, E.M., Cardine, A.M., Schraven, B., Brandt, R., Trotter, J., 2002. Process outgrowth of oligodendrocytes is promoted by interaction of fyn kinase with the cytoskeletal protein tau. J. Neurosci. 22, 698–707.

Klugmann, M., Schwab, M.H., Puhlhofer, A., Schneider, A., Zimmermann, F., Griffiths, I.R., Nave, K.A., 1997. Assembly of CNS myelin in the absence of proteolipid protein. Neuron 18, 59–70.

Koegl, M., Zlatkine, P., Ley, S.C., Courtneidge, S.A., Magee, A.I., 1994. Palmitoylation of multiple Src-family kinases at a homologous N-terminal motif. Biochem. J. 303 (Pt. 3), 749–753.

Kramer, E.M., Klein, C., Koch, T., Boytinck, M., Trotter, J., 1999. Compartmentation of Fyn kinase with glycosylphosphatidylinositol-anchored molecules in oligodendrocytes facilitates kinase activation during myelination. J. Biol. Chem. 274, 29042–29049.

Krueger, W.H., Gonye, G.E., Madison, D.L., Murray, K.E., Kumar, M., Spoerel, N., Pfeiffer, S.E., 1997. TPO1, a member of a novel protein family, is developmentally regulated in cultured oligodendrocytes. J. Neurochem. 69, 1343–1355.

Kyte, J., Doolittle, R.F., 1982. A simple method for displaying the hydropathic character of a protein. J. Mol. Biol. 157, 105–132.

Li, C., Tropak, M.B., Gerlai, R., Clapoff, S., Abramow-Newerly, W., Trapp, B., Peterson, A., Roder, J., 1994. Myelination in the absence of myelin-associated glycoprotein. Nature 369, 747–750.

Liang, X., Draghi, N.A., Resh, M.D., 2004. Signaling from integrins to Fyn to Rho family GTPases regulates morphologic differentiation of oligodendrocytes. J. Neurosci. 24, 7140–7149.

Lupski, J.R., de Oca-Luna, R.M., Slaugenhaupt, S., Pentao, L., Guzzetta, V., Trask, B.J., Saucedo-Cardenas, O., Barker, D.F., Killian, J.M., Garcia, C.A., et al., 1991. DNA duplication associated with Charcot–Marie–Tooth disease type 1A. Cell 66, 219–232.

Macklin, W.B., Weill, C.L., Deininger, P.L., 1986. Expression of myelin proteolipid and basic protein mRNAs in cultured cells. J. Neurosci. Res. 16, 203–217.

Marta, C.B., Taylor, C.M., Cheng, S., Quarles, R.H., Bansal, R., Pfeiffer, S.E., 2004. Myelin associated glycoprotein cross-linking triggers its partitioning into lipid rafts, specific signaling events and cytoskeletal rearrangements in oligodendrocytes. Neuron Glia Biology 1, 35–46.

Matsuda, Y., Koito, H., Yamamoto, H., 1997. Induction of myelin-associated glycoprotein expression through neuron-oligodendrocyte contact. Brain Res. Dev. Brain Res. 100, 110–116.

Mu, F.T., Callaghan, J.M., Steele-Mortimer, O., Stenmark, H., Parton, R.G., Campbell, P.L., McCluskey, J., Yeo, J.P., Tock, E.P., Toh, B.H., 1995. EEA1, an early endosome-associated protein. EEA1 is a conserved alpha-helical peripheral membrane protein flanked by cysteine "fingers" and contains a calmodulin-binding IQ motif. J. Biol. Chem. 270, 13503–13511.

Nakahara, J., Tan-Takeuchi, K., Seiwa, C., Gotoh, M., Kaifu, T., Ujike, A., Inui, M., Yagi, T., Ogawa, M., Aiso, S., Takai, T., Asou, H., 2003. Signaling via immunoglobulin Fc receptors induces oligodendrocyte precursor cell differentiation. Dev. Cell 4, 841–852.

Nakamura, N., Rabouille, C., Watson, R., Nilsson, T., Hui, N., Slusarewicz, P., Kreis, T.E., Warren, G., 1995. Characterization of a cis-Golgi matrix protein, GM130. J. Cell Biol. 131, 1715–1726.

Nakashima, K., Yanagisawa, M., Arakawa, H., Kimura, N., Hisatsune, T., Kawabata, M., Miyazono, K., Taga, T., 1999. Synergistic signaling in fetal brain by STAT3–Smad1 complex bridged by p300. Science 284, 479–482.

Osterhout, D.J., Wolven, A., Wolf, R.M., Resh, M.D., Chao, M.V., 1999. Morphological differentiation of oligodendrocytes requires activation of Fyn tyrosine kinase. J. Cell Biol. 145, 1209–1218.

Sakai, Y., Nakabayashi, O., Kikuchi, T., Wada, K., 1999. Identification of break points in mutated PMP22 gene in a new Trembler (Tr-Ncnp) mouse. Neuroscience 88, 989–991.

Sakamoto, Y., Kitamura, K., Yoshimura, K., Nishijima, T., Uyemura, K., 1987. Complete amino acid sequence of PO protein in bovine peripheral nerve myelin. J. Biol. Chem. 262, 4208–4214.

Schneider, A., Lander, H., Schulz, G., Wolburg, H., Nave, K.A., Schulz, J.B., Simons, M., 2005. Palmitoylation is a sorting determinant for transport to the myelin membrane. J. Cell Sci. 118, 2415–2423.

Scolding, N.J., Frith, S., Linington, C., Morgan, B.P., Campbell, A.K., Compston, D.A., 1989. Myelin-oligodendrocyte glycoprotein (MOG) is a surface marker of oligodendrocyte maturation. J. Neuroimmunol. 22, 169–176.

Shenoy-Scaria, A.M., Gauen, L.K., Kwong, J., Shaw, A.S., Lublin, D.M., 1993. Palmitylation of an amino-terminal cysteine motif of protein tyrosine kinases p56lck and p59fyn mediates interaction with glycosyl-phosphatidylinositol-anchored proteins. Mol. Cell. Biol. 13, 6385–6392.

Shy, M.E., Garbern, J.Y., Kamholz, J., 2002. Hereditary motor and sensory neuropathies: a biological perspective. Lancet Neurol. 1, 110–118.

Simons, K., Ikonen, E., 1997. Functional rafts in cell membranes. Nature 387, 569–572.

Sperber, B.R., McMorris, F.A., 2001. Fyn tyrosine kinase regulates oligodendroglial cell development but is not required for morphological differentiation of oligodendrocytes. J. Neurosci. Res. 63, 303–312.

Suh, J.G., Ichihara, N., Saigoh, K., Nakabayashi, O., Yamanishi, T., Tanaka, K., Wada, K., Kikuchi, T., 1997. An in-frame deletion in peripheral myelin protein-22 gene causes hypomyelination and cell death of the Schwann cells in the new Trembler mutant mice. Neuroscience 79, 735–744.

Suter, U., Welcher, A.A., Ozcelik, T., Snipes, G.J., Kosaras, B., Francke, U., Billings-Gagliardi, S., Sidman, R.L., Shooter, E.M., 1992. Trembler mouse carries a point mutation in a myelin gene. Nature 356, 241–244.

Takeuchi, M., Kuramochi, S., Fusaki, N., Nada, S., Kawamura-Tsuzuku, J., Matsuda, S., Semba, K., Toyoshima, K., Okada, M., Yamamoto, T., 1993. Functional and physical interaction of protein-tyrosine kinases Fyn and Csk in the T-cell signaling system. J. Biol. Chem. 268, 27413–27419.

Umemori, H., Sato, S., Yagi, T., Aizawa, S., Yamamoto, T., 1994. Initial events of myelination involve Fyn tyrosine kinase signalling. Nature 367, 572–576.

Umemori, H., Kadowaki, Y., Hirosawa, K., Yoshida, Y., Hironaka, K., Okano, H., Yamamoto, T., 1999. Stimulation of myelin basic protein gene transcription by Fyn tyrosine kinase for myelination. J. Neurosci. 19, 1393–1397.

Vallat, J.M., Sindou, P., Garbay, B., Preux, P.M., Anani, T., Richard, L., Diot, M., 1999. Expression of myelin proteins in the adult heterozygous Trembler mouse. Acta Neuropathol. (Berl.) 98, 281–287.

Vaux, D., Tooze, J., Fuller, S., 1990. Identification by anti-idiotype antibodies of an intracellular membrane protein that recognizes a mammalian endoplasmic reticulum retention signal. Nature 345, 495–502.

Verkade, P., Simons, K., 1997. Robert Feulgen Lecture 1997. Lipid microdomains and membrane trafficking in mammalian cells. Histochem. Cell Biol. 108, 211–220.

Weissert, R., Wallstrom, E., Storch, M.K., Stefferl, A., Lorentzen, J., Lassmann, H., Linington, C., Olsson, T., 1998. MHC haplotype-dependent regulation of MOG-induced EAE in rats. J. Clin. Invest. 102, 1265–1273.

Wolven, A., Okamura, H., Rosenblatt, Y., Resh, M.D., 1997. Palmitoylation of p59fyn is reversible and sufficient for plasma membrane association. Mol. Biol. Cell 8, 1159–1173.

Wong, M.H., Saam, J.R., Stappenbeck, T.S., Rexer, C.H., Gordon, J.I., 2000. Genetic mosaic analysis based on Cre recombinase and navigated laser capture microdissection. Proc. Natl. Acad. Sci. U. S. A. 97, 12601–12606.

THE JOURNAL OF BIOLOGICAL CHEMISTRY VOL. 281, NO. 41, pp. 30524–30533, October 13, 2006

Degradation of Amyotrophic Lateral Sclerosis-linked Mutant Cu,Zn-Superoxide Dismutase Proteins by Macroautophagy and the Proteasome*[S]

Received for publication, April 7, 2006, and in revised form, August 18, 2006 Published, JBC Papers in Press, August 18, 2006, DOI 10.1074/jbc.M603337200

Tomohiro Kabuta, Yasuyuki Suzuki, and Keiji Wada[1]

From the Department of Degenerative Neurological Diseases, National Institute of Neuroscience, National Center of Neurology and Psychiatry, Kodaira, Tokyo 187-8502, Japan

Mutations in the Cu,Zn-superoxide dismutase (SOD1) gene cause ~20% of familial cases of amyotrophic lateral sclerosis (fALS). Accumulating evidence indicates that a gain of toxic function of mutant SOD1 proteins is the cause of the disease. It has also been shown that the ubiquitin-proteasome pathway plays a role in the clearance and toxicity of mutant SOD1. In this study, we investigated the degradation pathways of wild-type and mutant SOD1 in neuronal and nonneuronal cells. We provide here the first evidence that wild-type and mutant SOD1 are degraded by macroautophagy as well as by the proteasome. Based on experiments with inhibitors of these degradation pathways, the contribution of macroautophagy to mutant SOD1 clearance is comparable with that of the proteasome pathway. Using assays that measure cell viability and cell death, we observed that under conditions where expression of mutant SOD1 alone does not induce toxicity, macroautophagy inhibition induced mutant SOD1-mediated cell death, indicating that macroautophagy reduces the toxicity of mutant SOD1 proteins. We therefore propose that both macroautophagy and the proteasome are important for the reduction of mutant SOD1-mediated neurotoxicity in fALS. Inhibition of macroautophagy also increased SOD1 levels in detergent-soluble and -insoluble fractions, suggesting that both detergent-soluble and -insoluble SOD1 are degraded by macroautophagy. These findings may provide further insights into the mechanisms of pathogenesis of fALS.

Amyotrophic lateral sclerosis (ALS)[2] is a neurodegenerative disease caused by selective loss of motor neurons (1, 2). Although most cases of ALS are sporadic, ~10% of ALS cases run in families. Dominant missense mutations in the gene that encodes the Cu,Zn-superoxide dismutase (SOD1) are responsible for 20% of familial ALS (fALS) cases (3). Mice overexpressing mutant SOD1 develop an ALS-like phenotype comparable with human ALS, whereas mice lacking SOD1 do not (4, 5). These findings have led to the conclusion that SOD1 mutants cause motor neuron degeneration by a toxic gain of function. Thus, studies of the degradation process of mutant SOD1 proteins could provide important insights into understanding the mechanisms that underlie the pathology of fALS, and possibly sporadic ALS, and into developing novel therapies for fALS by removing toxic species of mutant SOD1.

Cytoplasmic proteins are mainly degraded by two pathways, the ubiquitin-26 S proteasome pathway (6) and autophagy (7). Previous studies have shown that mutant SOD1 proteins are turned over more rapidly than wild-type SOD1, and a proteasome inhibitor increases the level of mutant SOD1 proteins (8, 9). Dorfin and NEDL1, two distinct ubiquitin ligases, ubiquitinate mutant but not wild-type SOD1 (10, 11). These observations suggest that mutant SOD1 is degraded by the ubiquitin-26 S proteasome pathway and that the increased turnover of mutant SOD1 is mediated in part by this pathway. On the other hand, the 20 S proteasome, a component of the 26 S proteasome, can degrade proteins without a requirement for ubiquitination (12, 13). A recent study has found that metal-free forms of wild-type and mutant SOD1 are degraded by the 20 S proteasome *in vitro* (14).

Autophagy is an intracellular process that results in the degradation of cytoplasmic components inside lysosomes. At least three forms of autophagy have been described in mammalian cells: macroautophagy, microautophagy, and chaperone-mediated autophagy (7). Macroautophagy is the major and the most well studied form of autophagy; this process begins with a sequestration step, in which cytosolic components are engulfed by a membrane sac called the isolation membrane. This membrane results in a double membrane structure called the autophagosome, which fuses with the lysosome. The inner membrane of the autophagosome and its protein and organelle contents are degraded by lysosomal hydrolases. Recent reports have demonstrated that macroautophagy plays an important role in preventing neurodegeneration in mice (15, 16). Although macroautophagy can be induced by starvation, this

* This work was supported by grants-in-aid for scientific research from the Japan Society for the Promotion of Science; a research grant in a priority area of research from the Ministry of Education, Culture, Sports, Science, and Technology, Japan; grants-in-aid for scientific research from the Ministry of Health, Labor and Welfare, Japan; and the Program for Promotion of Fundamental Studies in Health Sciences of the National Institute of Biomedical Innovation, Japan. The costs of publication of this article were defrayed in part by the payment of page charges. This article must therefore be hereby marked "*advertisement*" in accordance with 18 U.S.C. Section 1734 solely to indicate this fact.

[S] The on-line version of this article (available at http://www.jbc.org) contains supplemental Figs. S1–S6.

[1] To whom correspondence should be addressed: Dept. of Degenerative Neurological Diseases, National Institute of Neuroscience, National Center of Neurology and Psychiatry, 4-1-1 Ogawahigashi, Kodaira, Tokyo 187-8502, Japan. Tel.: 81-42-346-1715; Fax: 81-42-346-1745; E-mail: wada@ncnp.go.jp.

[2] The abbreviations used are: ALS, amyotrophic lateral sclerosis; fALS, familial ALS; SOD1, Cu,Zn-superoxide dismutase(s); 3-MA, 3-methyladenine; siRNA, short interfering RNA; EGFP, enhanced green fluorescent protein; HA, hemagglutinin; MTS, 3-(4,5-dimethylthiazol-2-yl)-5-(3-carboxymethoxyphenyl)-2-(4-sulfophenyl)-2H-tetrazolium.

pathway may take place constitutively in mammals (17). In cultured cells, inhibition of macroautophagy does not alter enhanced green fluorescent protein (EGFP) levels (18) or glyceraldehyde-3-phosphate dehydrogenase protein levels,[3] suggesting that not all cytosolic proteins are degraded by macroautophagy. To date, however, there have been no reports of macroautophagy in mutant SOD1 clearance.

In this study, we investigated the pathway by which human wild-type SOD1 and the A4V, G85R, and G93A SOD1 mutants are degraded in neuronal and nonneuronal cells. We show that wild-type and mutant SOD1 proteins are degraded by both the proteasomal pathway and macroautophagy. The experiments with inhibitors of these degradation pathways suggested that mutant SOD1 are degraded more rapidly than wild-type SOD1 in part by macroautophagy and that the contribution of macroautophagy to mutant SOD1 clearance is approximately equal to that of the proteasome pathway. Macroautophagy decreases mutant SOD1 protein levels in both nonionic detergent-soluble and -insoluble fractions. In addition, we provide data indicating that macroautophagy has a role in mutant SOD1-mediated cell death.

EXPERIMENTAL PROCEDURES

Plasmid Constructs—The expression plasmids pcDNA3-hSOD1 containing wild-type, A4V, G85R, and G93A mutant SOD1 were kindly donated by Ryosuke Takahashi (Kyoto University, Kyoto, Japan) and Makoto Urushitani (Laval University, Quebec, Canada) (19). To construct a plasmid expressing human wild-type SOD1 with the HA tag at the carboxyl terminus of SOD1, HA-tagged SOD1 fragments were amplified by PCR using wild-type SOD1 cDNA (Open Biosystems, Huntsville, AL) as the template. The PCR products were digested with XhoI and NotI and cloned into an XhoI-NotI-digested pCI-neo vector (Promega, Madison, WI). The primers used were 5′-AAAACTCGAGCCGCCAAGATGGCGACGAAGGCCGTGTGCG-3′ and 5′-AAAAGCGGCCGCTTAAGCGTAATCTGGAACATCGTATGGGTATTGGGCGATCCCAATTACACCACA-3′. A plasmid expressing HA-tagged G93A SOD1 was generated using QuikChange site-directed mutagenesis kit (Stratagene, La Jolla, CA) according to the manufacturer's protocol. To construct a plasmid expressing fusion protein of green fluorescent protein and LC3, LC3 fragments were amplified by PCR using rat LC3 cDNA (Open Biosystems) as the template. The PCR products were digested with BglII and EcoRI and cloned into a BglII-EcoRI-digested pEGFP-C1 vector (Clontech). The primers used were 5′-ACTCAGATCTATGCCGTCCGAGAAGACCTTCAAA-3′ and 5′-TGCAGAATTCTTACACAGCCAGTGCTGTCCCGAA-3′. After construction, the DNA sequences of the plasmids were confirmed by DNA sequence analysis.

Cell Culture and Transfection—The mouse neuroblastoma cell line Neuro2a, the human neuroblastoma cell line SH-SY5Y, and the monkey kidney-derived cell line COS-7 were maintained in Dulbecco's modified Eagle's medium (Sigma) supplemented with 10% fetal calf serum (JRH Biosciences, Lenexa, KS). Transient expression of each vector in Neuro2a and COS-7 cells was performed using the FuGENE 6 transfection reagent (Roche Applied Science). For experiments with differentiated Neuro2a cells, the medium was changed to differentiation medium (Dulbecco's modified Eagle's medium supplemented with 1% fetal calf serum and 20 μM retinoic acid) 24 h after transfection. Approximately 90% of cells in dishes (wells) were transfected in our experimental conditions (data not shown), and there was no notable differences in the transfection efficiency among the wells (supplemental Fig. S1).

Treatment of Cells with Epoxomicin, 3-Methyladenine, Cycloheximide, Rapamycin, or NH_4Cl—Cells grown in 12- or 6-well plates to 50–80% confluence were transfected with expression plasmids containing wild-type, A4V, G85R, or G93A mutant SOD1. 24 h after transfection, cells were incubated with epoxomicin (10 nM, 1 μM, 5 μM, or 10 μM; Sigma), 3-methyladenine (3-MA) (10, 20, or 30 mM; Sigma), rapamycin (100 or 200 nM; Sigma), 20 mM NH_4Cl, and/or carrier (Me_2SO or water) as a control. In some experiments, 10 μg/ml cycloheximide (Sigma) was added to the cells to avoid the confounding effects of ongoing protein synthesis. Epoxomicin, cycloheximide, and rapamycin were dissolved in Me_2SO, NH_4Cl in water. 3-MA was freshly dissolved in culture medium 30 min before use.

Cell Fractionation—For preparation of nonionic detergent-soluble and -insoluble fractions, adherent cells were harvested and lysed on ice for 15 min in 1% Triton X-100 lysis buffer containing 50 mM Tris-HCl, pH 7.5, 150 mM NaCl, 5 mM EDTA, 1% Triton X-100, and protease inhibitors (Complete, EDTA-free; Roche Applied Science). Lysates were centrifuged at 20,000 × *g* for 10 min at 4 °C, and the supernatants were pooled and designated as the detergent-soluble fractions. After the pellets were washed with 1% Triton X-100 lysis buffer, they were solubilized with SDS buffer (50 mM Tris-HCl, pH 7.5, 150 mM NaCl, 5 mM EDTA, 3% SDS, 1% Triton X-100, and protease inhibitors) and sonicated. The resulting solution was used as the detergent-insoluble fraction. For preparation of total cell lysates containing both detergent-soluble and -insoluble fractions, cells were lysed in SDS buffer and sonicated. Protein concentrations were determined with the protein assay kit (Bio-Rad) or the DC protein assay kit (Bio-Rad).

Western Blot Analysis—Western blotting was performed using standard procedures as described previously (20). The primary antibodies used were as follows: anti-SOD1 rabbit polyclonal antibody (1:4000; Stressgen Bioreagents, Victoria, Canada), anti-α-tubulin mouse monoclonal antibody (1:4000; Sigma), anti-β-actin mouse monoclonal antibody (1:5000; Sigma), anti-HA mouse monoclonal antibody (1:4000; Sigma), anti-Beclin 1 mouse monoclonal antibody (1:500; BD Transduction Laboratories, San Diego, CA), anti-Apg7/Atg7 rabbit polyclonal antibody (1:500; Rockland, Gilbertsville, PA). After overnight incubation with primary antibodies at 4 °C, each blot was probed with horseradish peroxidase-conjugated anti-rabbit IgG or anti-mouse IgG (1:20,000; Pierce). Immunoreactive signals were visualized with SuperSignal West Dura extended duration substrate (Pierce) or SuperSignal West Femto maximum sensitivity substrate (Pierce) and detected with a chemiluminescence imaging system (FluorChem; Alpha Innotech, San Leandro, CA). The signal intensity was quantified by densitometry using FluorChem software (Alpha Innotech).

Short Interfering RNA (siRNA) Preparation and Transfection—Double-stranded siRNA targeting mouse Beclin 1, mouse Atg7 and EGFP were purchased from RNAi Co., Ltd.

[3] T. Kabuta, Y. Suzuki, and K. Wada, unpublished data.

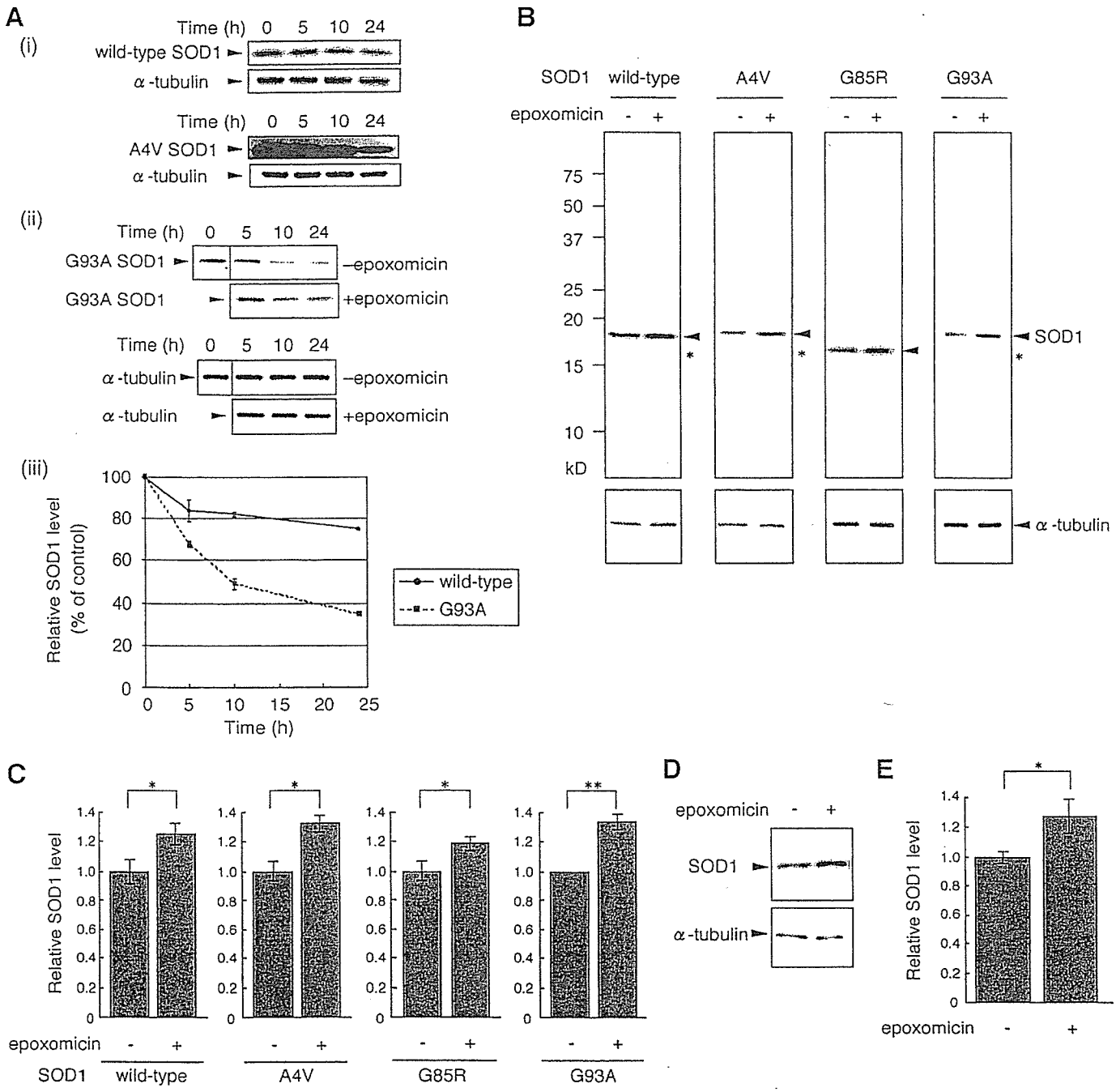

FIGURE 1. **Both mutant and wild-type SOD1 are degraded by the proteasome.** *A, i,* Neuro2a cells were transiently transfected with wild-type or mutant A4V human SOD1. 24 h after transfection, cells were treated with 10 μg/ml cycloheximide for the indicated time and lysed. Total cell lysates were analyzed by immunoblotting using anti-SOD1 or anti-α-tubulin antibody. *ii,* Neuro2a cells transfected with G93A SOD1 were incubated with or without 10 nM epoxomicin in the presence of 10 μg/ml cycloheximide for the indicated time and lysed. Total cell lysates were analyzed by immunoblotting using anti-SOD1 or anti-α-tubulin antibody. *iii,* the relative levels of wild-type or G93A SOD1 (percentage of 0-h control) were quantified by densitometry. Mean values are shown with S.E. ($n = 3$). *B* and *C,* Neuro2a cells were transiently transfected with wild-type or mutant A4V, G85R, or G93A human SOD1. 24 h after transfection, cells were incubated with or without 10 nM epoxomicin in the presence of 10 μg/ml cycloheximide for 24 h. Total cell lysates were analyzed by immunoblotting using anti-SOD1 antibody. The electrophoretic mobility of G85R SOD1 was greater than that of wild-type SOD1. α-Tubulin was used as a loading control. *Asterisks* indicate endogenous mouse SOD1 (*B*). The relative level of wild-type or mutant SOD1 was quantified by densitometry. Mean values are shown with S.E. ($n = 3$). *, $p < 0.05$; **, $p < 0.01$ (*C*). *D* and *E,* human SH-SY5Y cells were incubated with or without 10 nM epoxomicin in the presence of cycloheximide for 24 h. Total cell lysates were analyzed by immunoblotting with anti-SOD1 antibody (*D*). The relative level of human endogenous SOD1 was quantified by densitometry. Data are expressed as the means ± S.E. ($n = 3$). *, $p < 0.05$ (*E*).

(Tokyo, Japan). Sequences targeted by siRNA were selected using siDirect (RNAi Co., Ltd.): mouse Beclin 1 siRNA, sense (5′-GUCUACAGAAAGUGCUAAUAG-3′) and antisense (5′-AUUAGCACUUUCUGUAGACAU-3′); mouse Atg7 siRNA, sense (5′-GAGCGGCGGCUGGUAAGAACA-3′) and antisense (5′-UUCUUACCAGCCGCCGCUCAA-3′); EGFP siRNA, sense (5′-GCCACAACGUCUAUAUCAUGG-3′) and antisense (5′-AUGAUAUAGACGUUGUGGCUG-3′). EGFP siRNA was used as a control. Cells (3×10^5) were cotransfected with 1 μg of DNA and 3 μg of siRNA using Lipofectamine PLUS reagent (Invitrogen).

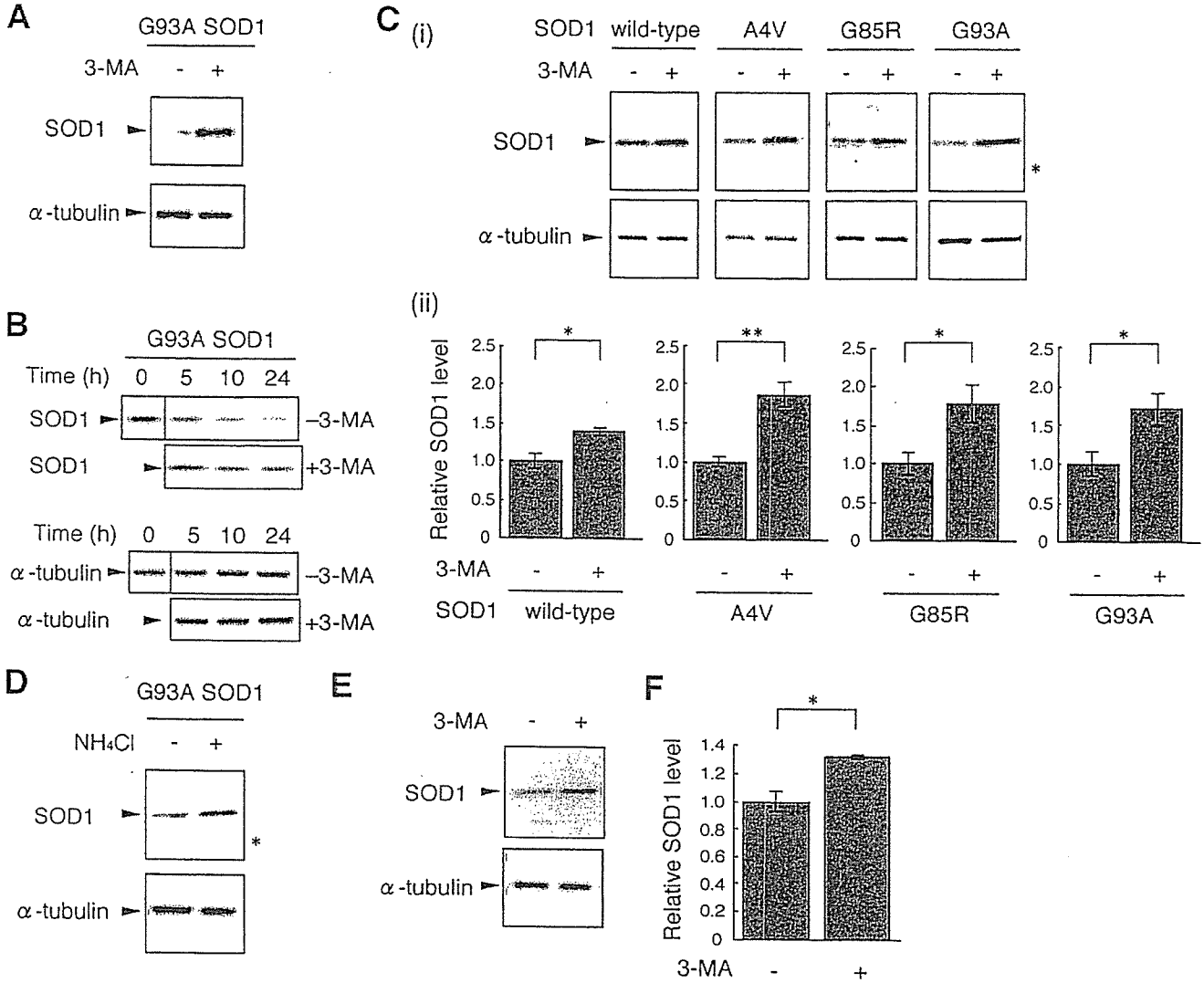

FIGURE 2. **Wild-type and mutant SOD1 are degraded by macroautophagy.** *A*, Neuro2a cells were transiently transfected with the G93A mutant SOD1. 24 h after transfection, cells were incubated with or without 10 mM 3-MA for 24 h. Total cell lysates were analyzed by immunoblotting using anti-SOD1 antibody. α-Tubulin was used as a loading control. *B*, Neuro2a cells transfected with G93A SOD1 were incubated with or without 10 mM 3-MA in the presence of 10 μg/ml cycloheximide for the indicated time and lysed. Total cell lysates were analyzed by immunoblotting using anti-SOD1 or anti-α-tubulin antibody. *C*, Neuro2a cells transfected with wild-type or mutant A4V, G85R, or G93A SOD1 were incubated with or without 10 mM 3-MA in the presence of 10 μg/ml cycloheximide for 24 h. Total cell lysates were analyzed by immunoblotting. An *asterisk* indicates endogenous mouse SOD1 (*i*). The relative level of wild-type or mutant SOD1 was quantified by densitometry. Mean values are shown with S.E. ($n = 3$): *, $p < 0.05$; **, $p < 0.01$ (*ii*). *D*, Neuro2a cells transfected with G93A SOD1 were incubated with or without 20 mM NH_4Cl in the presence of cycloheximide for 24 h. Total cell lysates were analyzed by immunoblotting. An *asterisk* indicates endogenous mouse SOD1. *E* and *F*, SH-SY5Y cells were incubated with or without 10 mM 3-MA in the presence of cycloheximide for 24 h. Total cell lysates were analyzed by immunoblotting (*E*). The relative level of human endogenous SOD1 was quantified by densitometry. Data are expressed as the means ± S.E. ($n = 3$). *, $p < 0.05$ (*F*).

Quantitative Assessment of Cell Viability and Cell Death—One day before transfection, Neuro2a cells were seeded at 5×10^4 cells/well in 24-well plates. 24 h after transfection with 0.4 μg of DNA/well, cells were cultured in differentiation medium with or without 10 mM 3-MA for 24 h. Cell death was assessed by a lactate dehydrogenase release assay using the CytoTox-ONE homogeneous membrane integrity assay (Promega) according to the manufacturer's protocol. The percentage of cytotoxicity (Fig. 7*G*) was calculated according to this protocol. For assessment of cell viability, we used the 3-(4,5-dimethylthiazol-2-yl)-5-(3-carboxymethoxyphenyl)-2-(4-sulfophenyl)-2H-tetrazolium (MTS) assay and the ATP assay with the CellTiter 96 AQueous One Solution cell proliferation assay (Promega) and CellTiter-Glo luminescent cell viability assay (Promega), respectively, according to the manufacturer's protocols. Measurements with a multiple-plate reader were performed after samples were transferred to 96-well assay plates.

Statistical Analysis—For comparison of two groups, the statistical difference was determined by Student's *t* test. For comparison of more than two groups, analysis of variance was used. If the analysis of variance was significant, Dunnett's multiple comparison test was used as a *post hoc* test.

RESULTS

Wild-type and Mutant SOD1 Are Degraded by the Proteasome—To determine whether SOD1 is degraded by the proteasome pathway, we assessed the effect of proteasome inhibitors on SOD1 protein clearance. Peptide aldehydes, such as

MG132 or ALLN, and lactacystin are widely used proteasome inhibitors. However, peptide aldehydes also inhibit cathepsins and calpains, and lactacystin inhibits cathepsin A (21, 22). Because these inhibitors are not proteasome-specific and may interfere with lysosomal function, we used epoxomicin as a selective proteasome inhibitor (23, 24). We observed protein clearance of human SOD1 in Neuro2a cells transfected with mutant or wild-type SOD1 in the presence of the translation inhibitor cycloheximide (Fig. 1*A*, *i* and *ii*). Consistent with previous reports (9, 11), wild-type SOD1 exhibited a relatively long half-life (half-life of more than 24 h) compared with mutant SOD1 (~10 h; G93A) (Fig. 1*A*, *iii*). The degradation of wild-type and mutant SOD1 was suppressed by epoxomicin treatment (Fig. 1, *B* and *C*) (~14-h increase in half-life; G93A; Fig. 1*A*, *ii*). Our finding that mutant SOD1 is degraded by the proteasome is in agreement with previous reports (8, 9). To determine whether endogenous human wild-type SOD1 is also degraded by the proteasome, SOD1 clearance was examined using the human neuroblastoma SH-SY5Y cell line. The proteasome inhibitor treatment promoted the accumulation of human SOD1 proteins (Fig. 1, *D* and *E*). These results indicate that endogenous wild-type SOD1 is degraded by the proteasome, also consistent with a previous report (14).

Wild-type and Mutant SOD1 Are Also Degraded by Macroautophagy—To date, there have been no reports of macroautophagy participating in human SOD1 clearance. We therefore investigated whether wild-type or mutant SOD1 was degraded by macroautophagy using 3-MA, an inhibitor of macroautophagy (18, 25, 26), and ammonium chloride, an inhibitor of lysosomal proteolysis (26). We initially confirmed that 3-MA inhibits the formation of autophagosomes in Neuro2a cells using green fluorescent protein-LC3, a marker of autophagosomes (27) (supplemental Fig. S2). Moreover, we also showed that the clearance of α-synuclein, an established substrate for macroautophagy (28), was inhibited by 3-MA or ammonium chloride treatment (supplemental Fig. S3). Treatment of Neuro2a cells with 3-MA promoted the accumulation of G93A mutant SOD1 proteins (Fig. 2*A*). In the presence of cycloheximide, the degradation of wild-type and mutant SOD1 was suppressed by treatment with 3-MA (Fig. 2, *B* and *C*) (a more than 14-h increase in half-life; G93A, Fig. 2*B*), indicating that wild-type and mutant SOD1 are degraded by macroautophagy in these cells and that the accumulation of SOD1 proteins by 3-MA is not due to increased protein synthesis. These results, together with Fig. 1, suggest that mutant SOD1 are degraded more rapidly than wild-type SOD1 by macroautophagy (it is estimated that 15–20% of wild-type SOD1 and 25–30% of mutant SOD1 were degraded by macroautophagy during the 24-h incubation). The clearance of mutant G93A SOD1 was also decreased by treatment with ammonium chloride (Fig. 2*D*). As shown in Supplemental Fig. S4 and Fig. 2*D*, the protein level of endogenous mouse SOD1 was increased by 3-MA or ammonium chloride treatment. The result shown in Fig. 2*D* further supports the role of the lysosomes in SOD1 degradation. To test the role of macroautophagy on SOD1 degradation in differentiated neuronal cells or neurons, we also used differentiated Neuro2a cells. In differentiated Neuro2a cells, 3-MA increased both wild-type and mutant SOD1 protein levels in the presence or absence of

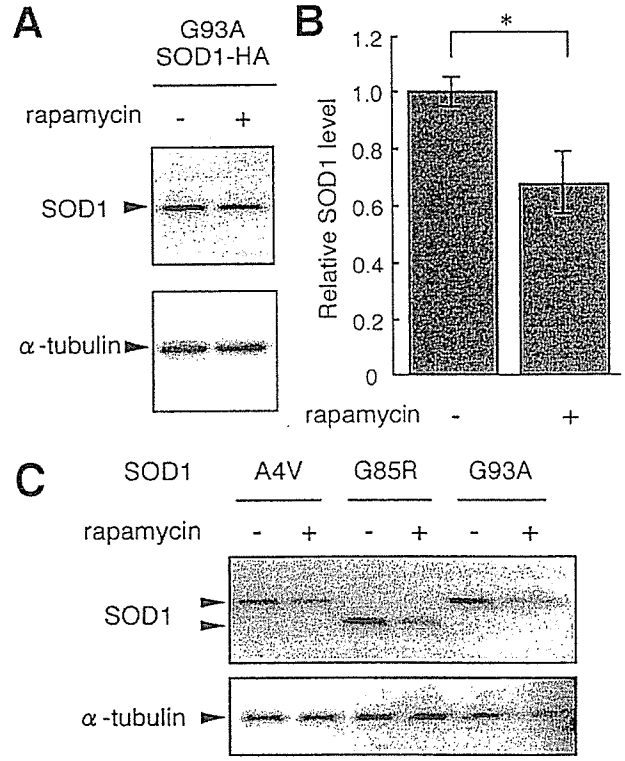

FIGURE 3. **Rapamycin treatment decreases mutant SOD1 protein levels.** *A* and *B*, Neuro2a cells were transiently transfected with HA-tagged G93A SOD1. 24 h after transfection, cells were incubated with or without 100 nM rapamycin for 24 h. Total cell lysates were analyzed by immunoblotting using anti-SOD1 antibody. α-Tubulin was used as a loading control (*A*). The relative level of mutant G93A SOD1 was quantified by densitometry. Data are presented as the means ± S.E. ($n = 3$). *, $p < 0.05$ (*B*). *C*, Neuro2a cells transfected with mutant A4V, G85R, or G93A SOD1 were cultured in differentiation medium with or without 200 nM rapamycin for 24 h. Total cell lysates were analyzed by immunoblotting.

cycloheximide (data not shown). To determine whether endogenous human SOD1 is degraded by macroautophagy, the clearance of endogenous SOD1 was examined in SH-SY5Y cells. As shown in Fig. 2, *E* and *F*, the degradation of endogenous SOD1 proteins was inhibited by 3-MA.

For further confirmation of the clearance of SOD1 by macroautophagy, we used rapamycin to induce macroautophagy (29, 30), and gene silencing with siRNA to inhibit macroautophagy. Treating Neuro2a cells with rapamycin decreased HA-tagged G93A SOD1 levels (Fig. 3, *A* and *B*). In differentiated Neuro2a cells, SOD1 protein levels were also decreased by rapamycin (Fig. 3*C*). Beclin 1 is a component of a class III phosphatidylinositol 3-kinase complex that is crucial for macroautophagy (31). Silencing of the Beclin 1 gene by siRNA inhibits the generation of autophagosomes, thus preventing macroautophagy (32). Atg7 protein is also essential for macroautophagy (17). We initially confirmed that Beclin 1 or Atg7 expression was knocked down by Beclin 1 or Atg7 siRNA, respectively (Fig. 4, *A* and *B*). We also showed that α-synuclein level was increased by Beclin 1 or Atg7 siRNA (supplemental Fig. S3). We observed inhibited degradation of wild-type and mutant SOD1 in cells with Beclin 1 siRNA (Fig. 4, *A* and *C*) or Atg7 siRNA (Fig. 4, *B* and *D*) compared with cells with control siRNA (~14 h increase in half-life; G93A; Fig. 4*E*). The results shown in Figs. 2–4 demonstrate that wild-type and mutant SOD1 are also

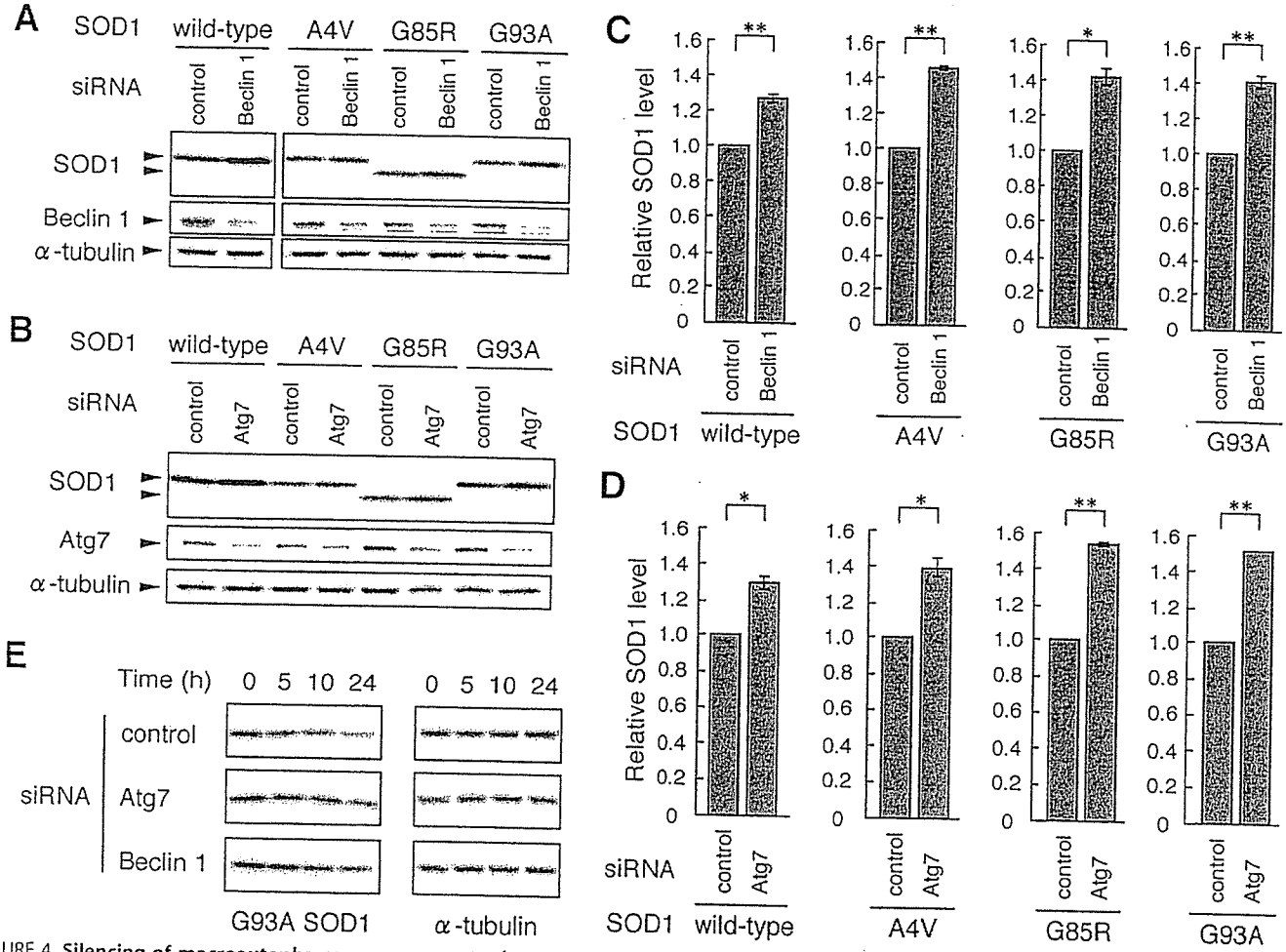

FIGURE 4. **Silencing of macroautophagy genes promote the accumulation of SOD1 proteins.** *A* and *C*, Neuro2a cells were cotransfected with SOD1 (wild-type, A4V, G85R, or G93A) and siRNA (Beclin 1 siRNA or control EGFP siRNA). 24 h after transfection, total cell lysates were prepared and analyzed by immunoblotting using anti-SOD1 or anti-Beclin 1 antibody. α-Tubulin was used as a control (*A*). Levels of SOD1 were quantified by densitometry, and the levels are expressed as -fold level of SOD1 in cells with Beclin 1 siRNA over cells with control siRNA. Data are presented as the means ± S.E. ($n = 3$). *, $p < 0.05$; **, $p < 0.01$ (*C*). *B* and *D*, Neuro2a cells were cotransfected with SOD1 (wild-type, A4V, G85R, or G93A) and siRNA (Atg7 siRNA or control siRNA). 24 h after transfection, total cell lysates were prepared and analyzed by immunoblotting using anti-SOD1, anti-Atg7, or anti-α-tubulin antibody (*B*). Levels of SOD1 were quantified by densitometry, and the levels are expressed as -fold level of SOD1 in cells with Atg7 siRNA over cells with control siRNA. Data are presented as the means ± S.E. ($n = 3$). *, $p < 0.05$; **, $p < 0.01$ (*D*). *E*, Neuro2a cells cotransfected with G93A SOD1 and siRNA (control, Atg7, or Beclin 1 siRNA) were treated with 10 μg/ml cycloheximide for the indicated time and lysed. Total cell lysates were analyzed by immunoblotting using anti-SOD1 or anti-α-tubulin antibody.

degraded by macroautophagy in neuronal cells. In the nonneuronal COS-7 cells, ammonium chloride or 3-MA treatment stimulated the accumulation of HA-tagged wild-type SOD1 and G93A SOD1 (Fig. 5*A*) or mutant G93A SOD1 (Fig. 5*B*), respectively. Treatment of the cells with epoxomicin also increased wild-type and mutant SOD1 levels (Fig. 5*C* and supplemental Fig. S5). These results indicate that wild-type and mutant SOD1 are degraded by both macroautophagy and the proteasome in COS-7 cells. The results shown in Figs. 3*A* and 5*A* indicate that not only SOD1 without a tag but also HA-tagged SOD1 is degraded by macroautophagy.

The Contributions of the Proteasome Pathway and Macroautophagy to Mutant SOD1 Degradation Are Comparable—We then assessed the relative contributions of proteasomal degradation and macroautophagy to the clearance of mutant SOD1. As shown in Fig. 6*A*, 10 mM 3-MA entirely suppresses the (3-MA-sensitive) macroautophagy-mediated degradation of mutant SOD1. 1 μM epoxomicin also entirely suppresses the (epoxomicin-sensitive) proteasome-mediated degradation of mutant SOD1 (Fig. 6*B* and supplemental Fig. S6). Therefore, we compared mutant G93A SOD1 levels in 1 μM epoxomicin-treated cells with that of 10 mM 3-MA-treated cells. The SOD1 protein level in 3-MA-treated cells was comparable with that of epoxomicin-treated cells (Fig. 6, *C–F*). An increased accumulation of mutant SOD1 was detected in cells cotreated with both inhibitors compared with that of 3-MA-treated cells or epoxomicin-treated cells (Fig. 6, *E* and *F*). These data further support the idea that mutant SOD1 proteins are degraded by both macroautophagy and the proteasome and indicate that, in these cells, the contribution of macroautophagy to mutant SOD1 clearance is approximately equal to that of the proteasome pathway.

Macroautophagy Reduces the Toxicity of Mutant SOD1—Previous studies have shown that mutant SOD1-expressing cells are more susceptible to cell death induced by proteasome inhibition (33). We examined whether inhibiting the macroautophagy-mediated degradation of mutant SOD1 could also induce cell death in Neuro2a cells using three different assays.

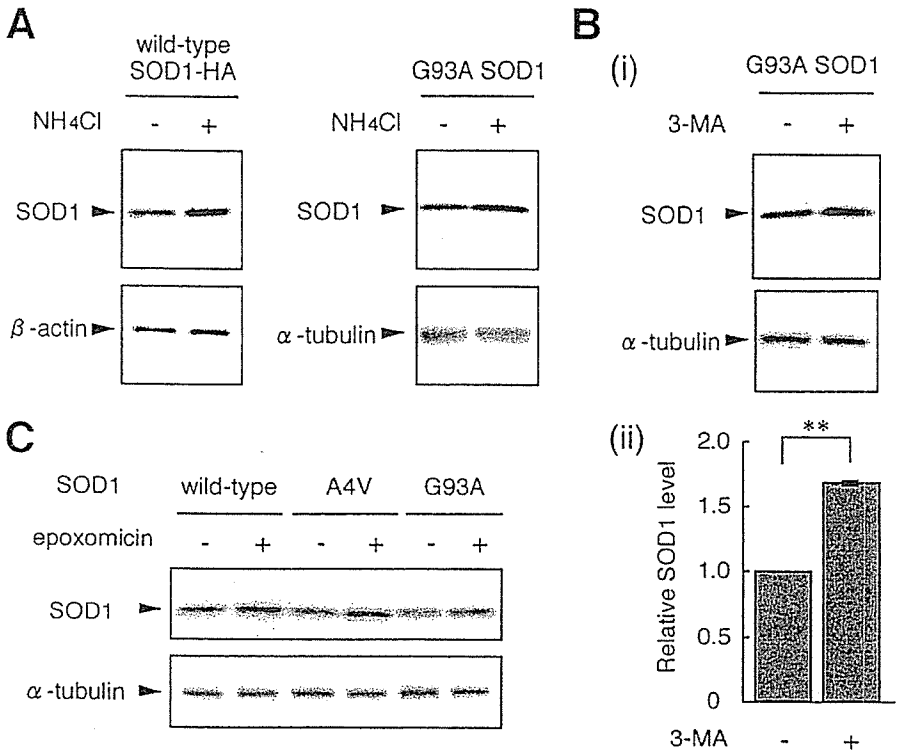

FIGURE 5. **Mutant and wild-type SOD1 are degraded by both macroautophagy and the proteasome in COS-7 cells.** *A*, COS-7 cells were transiently transfected with HA-tagged human wild-type SOD1 or G93A SOD1. 24 h after transfection, cells were incubated with or without 20 mM NH_4Cl for 24 h. Total cell lysates were analyzed by immunoblotting using anti-HA antibody or anti-SOD1 antibody. β-Actin and α-tubulin were used as loading controls. *B*, COS-7 cells transfected with G93A mutant SOD1 were incubated with or without 10 mM 3-MA in the presence of cycloheximide for 24 h. Total cell lysates were analyzed by immunoblotting using anti-SOD1 antibody (*i*). Levels of SOD1 were quantified by densitometry, and the levels are expressed as -fold level of SOD1 in cells with 3-MA over control. Data are presented as the means ± S.E. ($n = 3$). **, $p < 0.01$ (*ii*). *C*, COS-7 cells were transfected with wild-type or mutant A4V or G93A SOD1. 24 h after transfection, cells were incubated with or without 10 nM epoxomicin for 24 h. Total cell lysates were analyzed by immunoblotting.

For assessment of cell viability, we used the MTS assay and ATP assay, and for assessment of cell death, we used the lactate dehydrogenase release assay. In untreated differentiated Neuro2a cells, there was no statistically significant difference in cell viability or cell death among control cells, wild-type SOD1-expressing cells, and mutant SOD1-expressing cells (Fig. 7, *A–C*). However, when cells were treated with 3-MA, mutant SOD1-expressing cells showed significantly increased cell death and significantly decreased cell viability compared with control cells or wild-type SOD1-expressing cells (Fig. 7, *D–F*). When compared with cell death of 3-MA-untreated cells, cell death of 3-MA-treated cells was increased in mutant SOD1-expressed cells but not in cells with wild-type SOD1 (Fig. 7*G*). From these results, we conclude that macroautophagy reduces mutant SOD1-mediated toxicity in this cell model.

Inhibition of Macroautophagy Leads to Accumulation of both Detergent-soluble and Detergent-insoluble Mutant SOD1—Detergent-insoluble SOD1 proteins, aggregates, or inclusion bodies have been found in motor neurons in fALS patients (34), mouse models of fALS (35), and the cells transfected with mutant SOD1 (9, 36), although it is not clear whether these insoluble SOD1 proteins and aggregates are toxic because of conflicting results on the correlation between aggregate formation and cell death (36, 37). We investigated the effect of macroautophagy inhibition on the clearance of nonionic detergent-soluble and -insoluble SOD1. The nonionic detergent-soluble and -insoluble fractions were subjected to SDS-PAGE following Western blotting. In agreement with a previous report (9), mutant SOD1 proteins exhibited increased nonionic detergent insolubility compared with wild-type SOD1 (Fig. 8*B*). The increased level of wild-type SOD1 compared with mutant in the detergent-soluble fraction (Fig. 8*A*) is probably due to the rapid turnover of mutant SOD1. Incubation with 3-MA increased monomer SOD1 levels in the detergent-soluble (Fig. 8*A*) and -insoluble fractions (Fig. 8*B*), suggesting that both detergent-soluble and -insoluble SOD1 are degraded by macroautophagy. Consistent with a previous report (9), we found SDS-resistant dimers and high molecular weight aggregates of mutant SOD1 in the detergent-insoluble fraction (Fig. 8*C*). These dimers and aggregates of mutant SOD1 were increased by 3-MA treatment (Fig. 8*C*), suggesting that insoluble aggregates of mutant SOD1 are also cleared by macroautophagy. The results from Figs. 7 and 8 indicate that the accumulation of toxic mutant SOD1 proteins by macroautophagy inhibition leads to greater cell death.

DISCUSSION

Using inhibitors of macroautophagy and proteasomal degradation, we have shown that both wild-type and mutant SOD1 proteins are degraded by both pathways. Accumulating evidence has shown that mutant SOD1 is degraded by the ubiquitin-proteasome pathway (8, 9, 19). However, most of these studies have used lactacystin or a peptide aldehyde, both of which are not proteasome-specific inhibitors. Our data on the effect of the selective proteasome inhibitor epoxomicin also indicate that mutant SOD1 is degraded by the proteasome. Because wild-type SOD1 is not ubiquitinated by the ubiquitin ligases (10, 11), it has been proposed that wild-type SOD1 is not a substrate of the proteasome. However, a recent report has suggested that wild-type SOD1 can be degraded by the 20 S proteasome without ubiquitination (14). Moreover, we show here that epoxomicin treatment increases both overexpressed and endogenous wild-type SOD1 levels. Our data together with the previous reports support the idea that wild-type SOD1 is degraded by the 20 S proteasome in mammalian cells.

In this study, we demonstrated for the first time that macro-

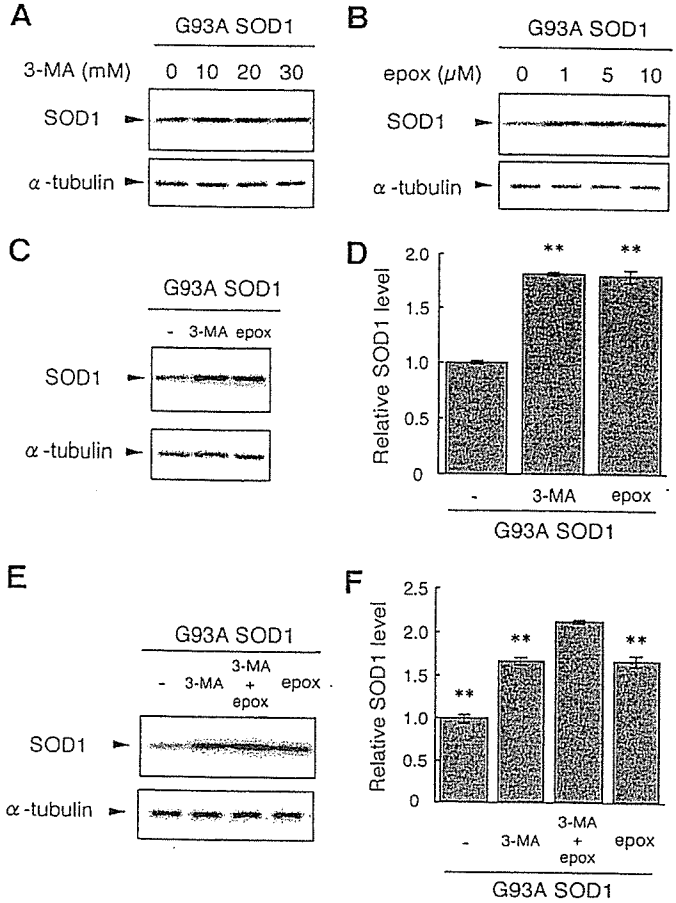

FIGURE 6. **The contribution of macroautophagy to SOD1 clearance is comparable with that of the proteasome.** *A*, Neuro2a cells transfected with mutant G93A SOD1 were incubated with or without 10, 20, or 30 mM 3-MA for 24 h. Total cell lysates were analyzed by immunoblotting. *B*, Neuro2a cells transfected with mutant G93A SOD1 were incubated with or without 1, 5, or 10 μM epoxomicin (*epox*) for 24 h. Total cell lysates were analyzed by immunoblotting. *C* and *D*, Neuro2a cells transfected with mutant G93A SOD1 were incubated with or without 10 mM 3-MA or 1 μM epoxomicin for 24 h. Total cell lysates were analyzed by immunoblotting (*C*). The relative level of mutant G93A SOD1 was quantified by densitometry. Data are presented as the means ± S.E. ($n = 3$). **, $p < 0.01$ in comparison with control (analysis of variance with Dunnett's multiple comparison test). (*D*). *E* and *F*, COS-7 cells transfected with mutant G93A SOD1 were incubated with or without 10 mM 3-MA, 1 μM epoxomicin, or both inhibitors (10 mM 3-MA and 1 μM epoxomicin) in the presence of cycloheximide for 24 h. Total cell lysates were analyzed by immunoblotting (*E*). The relative level of mutant G93A SOD1 was quantified by densitometry. Data are presented as the means ± S.E. ($n = 3$). **, $p < 0.01$ in comparison with 3-MA + epoxomicin (analysis of variance with Dunnett's multiple comparison test) (*F*).

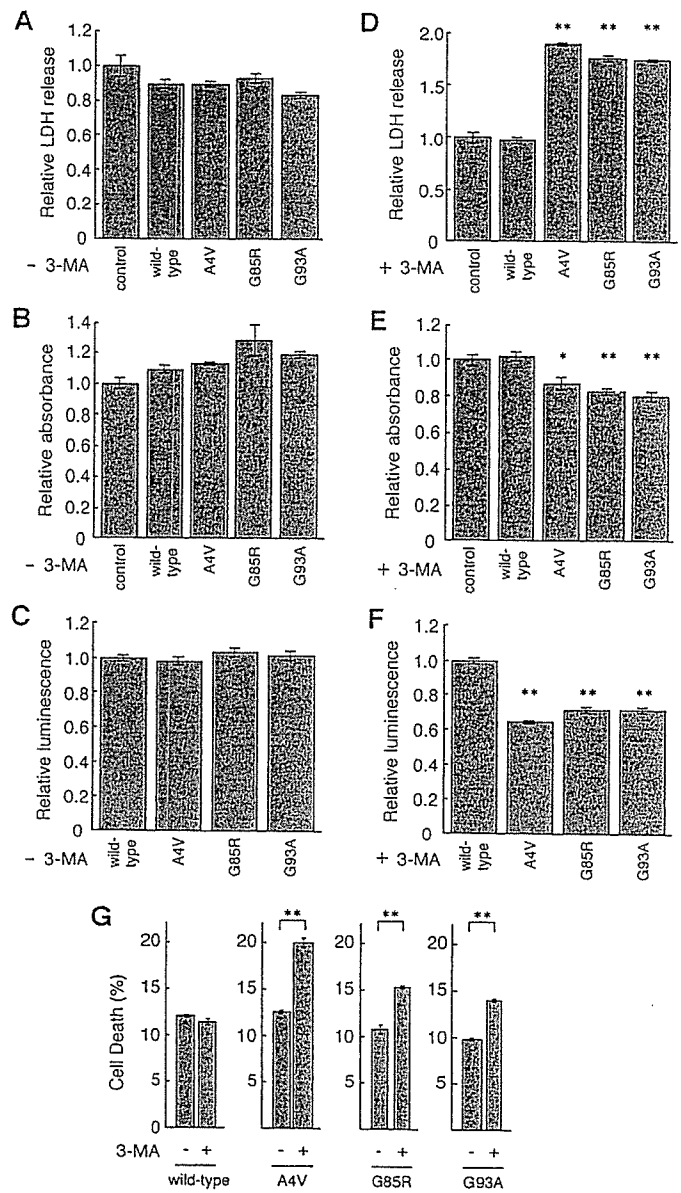

FIGURE 7. **Macroautophagy inhibition causes mutant SOD1-mediated cell death.** *A–G*, Neuro2a cells were transiently transfected with control empty vector (*A*, *B*, *D*, and *E*) or human SOD1 (wild type, A4V, G85R, or G93A). 24 h after transfection, cells were incubated in differentiation medium with (*D–G*) or without (*A–C* and *G*) 10 mM 3-MA for 24 h, and the lactate dehydrogenase release assay (*A*, *D*, and *G*), MTS assay (*B* and *E*), or ATP assay (*C* and *F*) were performed. The percentage of nonviable cells in each sample was calculated from the lactate dehydrogenase release assay (*G*). The experiment in *G* was performed independently of *A* and *D*. Data are expressed as the means ± S.E. ($n = 4$ in *A*, *C*, *D*, *F*, and *G*; $n = 3$ in *B* and *E*). *, $p < 0.05$; **, $p < 0.01$ in comparison with control (*A*, *B*, *D*, and *E*) or with wild-type SOD1 (*C* and *F*) (analysis of variance with Dunnett's multiple comparison test). **, $p < 0.01$ (*G*; *t* test).

autophagy is another pathway for degradation of wild-type and mutant SOD1. Our findings are consistent with a previous report that rat wild-type SOD1 is present in autophagosomes and lysosomes in rat hepatocytes (although they did not examine whether rat SOD1 was degraded by macroautophagy in those cells) (38). We propose that the contribution of macroautophagy to mutant SOD1 degradation is comparable with that of the proteasome pathway in the cell types we tested. Recent studies have demonstrated that transgenic mice with neuron-specific expression of mutant SOD1 do not exhibit an ALS-like phenotype (39, 40) and that neurodegeneration is delayed when motor neurons expressing mutant SOD1 are surrounded by healthy nonneuronal wild-type cells (41). In addition, Urushitani *et al.* (42) have shown that chromogranins promote secretion of mutant SOD1 from cells expressing the mutant protein, and they proposed that secreted mutant SOD1 can be toxic to neighboring cells. These studies strongly suggest that the expression of mutant SOD1 in nonneuronal cells may be involved in mutant SOD1-mediated neurotoxicity. In nonneuronal COS-7 cells, mutant SOD1 is also degraded by both the proteasome and macroautophagy (Fig. 5). Thus, not only the proteasome but also macroautophagy may play an important

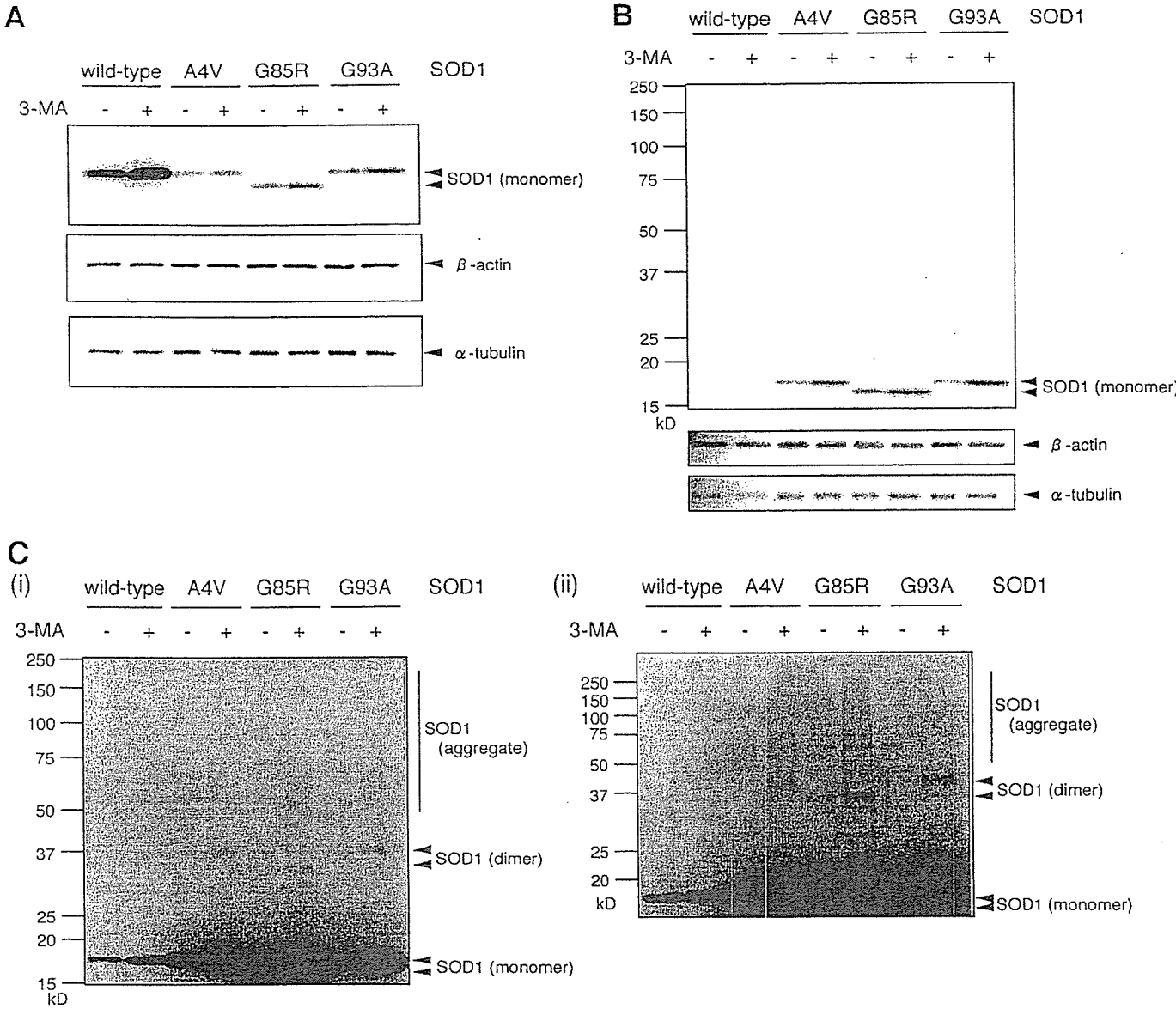

FIGURE 8. **Inhibition of macroautophagy causes accumulation of both detergent-soluble and -insoluble mutant SOD1.** *A–C*, Neuro2a cells were transiently transfected with human wild-type or mutant A4V, G85R, or G93A SOD1. 24 h after transfection, cells were cultured in differentiation medium with or without 10 mM 3-MA for 24 h. Triton X-100-soluble (*A*) and -insoluble (*B* and *C*) fractions were prepared and analyzed by immunoblotting using anti-SOD1 antibody. β-Actin and α-tubulin were used as loading controls. *C* (*i*), a longer exposure of *B*. *C* (*i* and *ii*), two different sets of experiments with longer exposure.

role in clearance of mutant SOD1 in fALS in nonneuronal cells as well as in neuronal cells.

It has been well established that mutant SOD1-mediated toxicity is caused by a gain of toxic function rather than the loss of SOD1 activity (1, 2). The appearance of mutant SOD1 aggregates in motor neurons in fALS patients and mouse models of fALS (34, 35) has suggested that aggregation has a role in neurotoxicity. However, conflicting results have been reported on the correlation between aggregate formation and cell death. A recent study has shown that the ability of mutant G85R and G93A SOD1 proteins to form aggregates correlates with neuronal cell death using live cell imaging techniques (36). Another report has concluded that aggregate formation of A4V and V148G SOD1 mutants does not correlate with cell death (37). These controversies also exist in other neurodegenerative diseases (43–46). Our current data suggest that macroautophagy degrades toxic species of mutant SOD1 and that the accumulation of mutant SOD1 proteins leads to greater cell death. However, whether the toxic SOD1 species are monomers, oligomers, or aggregates cannot be determined from our study, because a variety of mutant SOD1 species, including detergent-soluble SOD1 monomers and detergent-insoluble monomers, dimers, and aggregates, were accumulated by macroautophagy inhibition (Fig. 8).

Our data show that macroautophagy reduces mutant SOD1-mediated toxicity and that induction of macroautophagy decreases mutant SOD1 protein levels. Niwa *et al.* (10) have shown that the ubiquitin ligase Dorfin ubiquitinates mutant SOD1 and prevents the neurotoxicity of mutant SOD1. Taken together, these data imply that macroautophagy inducers, acti-

vators of the ubiquitin-proteasome pathway, or a combination of the two have therapeutic potential for fALS. In conclusion, our results demonstrate that mutant SOD1 is degraded by at least two pathways, macroautophagy and the proteasome pathway, and that the clearance of mutant SOD1 by macroautophagy reduces its cell toxicity. These findings may provide insight into the molecular mechanisms of the pathogenesis of fALS.

Acknowledgments—We thank Dr. Ryosuke Takahashi (Kyoto University) and Dr. Makoto Urushitani (Laval University) for the gift of pcDNA3-hSOD1 (wild-type and mutant A4V, G85R, and G93A) plasmids, and Naoki Takagaki for the support in English.

REFERENCES

1. Bruijn, L. I., Miller, T. M., and Cleveland, D. W. (2004) *Annu. Rev. Neurosci.* 27, 723–749
2. Cleveland, D. W., and Rothstein, J. D. (2001) *Nat. Rev. Neurosci.* 2, 806–819
3. Rosen, D. R., Siddique, T., Patterson, D., Figlewicz, D. A., Sapp, P., Hentati, A., Donaldson, D., Goto, J., O'Regan, J. P., Deng, H. X., Rahmani, Z., Krizus, A., McKenna-Yasek, D., Cayabyab, A., Gaston, S. M., Berger, R., Tanzi, R. E., Halperin, J. J., Herzfeldt, B., Van den Bergh, R., Hung, W. Y., Bird, T., Deng, G., Mulder, D. W., Smyth, C., Laing, N. G., Soriano, E., Pericak-Vance, M. A., Haines, J., Rouleau, G. A., Gusella, J. S., Horvitz, H. R., and Brown, R. H., Jr. (1993) *Nature* 362, 59–62
4. Gurney, M. E., Pu, H., Chiu, A. Y., Dal Canto, M. C., Polchow, C. Y., Alexander, D. D., Caliendo, J., Hentati, A., Kwon, Y. W., Deng, H. X., Chen, W., Zhai, P., Sufit, R. L., and Siddique, T. (1994) *Science* 264, 1772–1775
5. Reaume, A. G., Elliott, J. L., Hoffman, E. K., Kowall, N. W., Ferrante, R. J., Siwek, D. F., Wilcox, H. M., Flood, D. G., Beal, M. F., Brown, R. H., Jr., Scott, R. W., and Snider, W. D. (1996) *Nat. Genet.* 13, 43–47
6. Goldberg, A. L. (2003) *Nature* 426, 895–899
7. Cuervo, A. M. (2004) *Trends Cell Biol.* 14, 70–77
8. Hoffman, E. K., Wilcox, H. M., Scott, R. W., and Siman, R. (1996) *J. Neurol. Sci.* 139, 15–20
9. Johnston, J. A., Dalton, M. J., Gurney, M. E., and Kopito, R. R. (2000) *Proc. Natl. Acad. Sci. U. S. A.* 97, 12571–12576
10. Niwa, J., Ishigaki, S., Hishikawa, N., Yamamoto, M., Doyu, M., Murata, S., Tanaka, K., Taniguchi, N., and Sobue, G. (2002) *J. Biol. Chem.* 277, 36793–36798
11. Miyazaki, K., Fujita, T., Ozaki, T., Kato, C., Kurose, Y., Sakamoto, M., Kato, S., Goto, T., Itoyama, Y., Aoki, M., and Nakagawara, A. (2004) *J. Biol. Chem.* 279, 11327–11335
12. Shringarpure, R., Grune, T., Mehlhase, J., and Davies, K. J. (2003) *J. Biol. Chem.* 278, 311–318
13. Asher, G., Tsvetkov, P., Kahana, C., and Shaul, Y. (2005) *Genes Dev.* 19, 316–321
14. Di Noto, L., Whitson, L. J., Cao, X., Hart, P. J., and Levine, R. L. (2005) *J. Biol. Chem.* 280, 39907–39913
15. Komatsu, M., Waguri, S., Chiba, T., Murata, S., Iwata, J., Tanida, I., Ueno, T., Koike, M., Uchiyama, Y., Kominami, E., and Tanaka, K. (2006) *Nature* 441, 880–884
16. Hara, T., Nakamura, K., Matsui, M., Yamamoto, A., Nakahara, Y., Suzuki-Migishima, R., Yokoyama, M., Mishima, K., Saito, I., Okano, H., and Mizushima, N. (2006) *Nature* 441, 885–889
17. Komatsu, M., Waguri, S., Ueno, T., Iwata, J., Murata, S., Tanida, I., Ezaki, J., Mizushima, N., Ohsumi, Y., Uchiyama, Y., Kominami, E., Tanaka, K., and Chiba, T. (2005) *J. Cell Biol.* 169, 425–434
18. Ravikumar, B., Duden, R., and Rubinsztein, D. C. (2002) *Hum. Mol. Genet.* 11, 1107–1117
19. Urushitani, M., Kurisu, J., Tsukita, K., and Takahashi, R. (2002) *J. Neurochem.* 83, 1030–1042
20. Kabuta, T., Hakuno, F., Asano, T., and Takahashi, S. (2002) *J. Biol. Chem.* 277, 6846–6851
21. Lee, D. H., and Goldberg, A. L. (1998) *Trends Cell Biol.* 8, 397–403
22. Ostrowska, H., Wojcik, C., Wilk, S., Omura, S., Kozlowski, L., Stoklosa, T., Worowski, K., and Radziwon, P. (2000) *Int. J. Biochem. Cell Biol.* 32, 747–757
23. Meng, L., Mohan, R., Kwok, B. H., Elofsson, M., Sin, N., and Crews, C. M. (1999) *Proc. Natl. Acad. Sci. U. S. A.* 96, 10403–10408
24. Garcia-Echeverria, C. (2002) *Mini Rev. Med. Chem.* 2, 247–259
25. Qin, Z. H., Wang, Y., Kegel, K. B., Kazantsev, A., Apostol, B. L., Thompson, L. M., Yoder, J., Aronin, N., and DiFiglia, M. (2003) *Hum. Mol. Genet.* 12, 3231–3244
26. Cuervo, A. M., Stefanis, L., Fredenburg, R., Lansbury, P. T., and Sulzer, D. (2004) *Science* 305, 1292–1295
27. Kabeya, Y., Mizushima, N., Ueno, T., Yamamoto, A., Kirisako, T., Noda, T., Kominami, E., Ohsumi, Y., and Yoshimori, T. (2000) *EMBO J.* 19, 5720–5728
28. Webb, J. L., Ravikumar, B., Atkins, J., Skepper, J. N., and Rubinsztein, D. C. (2003) *J. Biol. Chem.* 278, 25009–25013
29. Blommaart, E. F., Luiken, J. J., Blommaart, P. J., van Woerkom, G. M., and Meijer, A. J. (1995) *J. Biol. Chem.* 270, 2320–2326
30. Gutierrez, M. G., Master, S. S., Singh, S. B., Taylor, G. A., Colombo, M. I., and Deretic, V. (2004) *Cell* 119, 753–766
31. Liang, X. H., Jackson, S., Seaman, M., Brown, K., Kempkes, B., Hibshoosh, H., and Levine, B. (1999) *Nature* 402, 672–676
32. Shimizu, S., Kanaseki, T., Mizushima, N., Mizuta, T., Arakawa-Kobayashi, S., Thompson, C. B., and Tsujimoto, Y. (2004) *Nat. Cell Biol.* 6, 1221–1228
33. Aquilano, K., Rotilio, G., and Ciriolo, M. R. (2003) *J. Neurochem.* 85, 1324–1335
34. Kato, S., Takikawa, M., Nakashima, K., Hirano, A., Cleveland, D. W., Kusaka, H., Shibata, N., Kato, M., Nakano, I., and Ohama, E. (2000) *Amyotroph. Lateral Scler. Other Motor Neuron Disord.* 1, 163–184
35. Bruijn, L. I., Becher, M. W., Lee, M. K., Anderson, K. L., Jenkins, N. A., Copeland, N. G., Sisodia, S. S., Rothstein, J. D., Borchelt, D. R., Price, D. L., and Cleveland, D. W. (1997) *Neuron* 18, 327–338
36. Matsumoto, G., Stojanovic, A., Holmberg, C. I., Kim, S., and Morimoto, R. I. (2005) *J. Cell Biol.* 171, 75–85
37. Lee, J. P., Gerin, C., Bindokas, V. P., Miller, R., Ghadge, G., and Roos, R. P. (2002) *J. Neurochem.* 82, 1229–1238
38. Rabouille, C., Strous, G. J., Crapo, J. D., Geuze, H. J., and Slot, J. W. (1993) *J. Cell Biol.* 120, 897–908
39. Pramatarova, A., Laganiere, J., Roussel, J., Brisebois, K., and Rouleau, G. A. (2001) *J. Neurosci.* 21, 3369–3374
40. Lino, M. M., Schneider, C., and Caroni, P. (2002) *J. Neurosci.* 22, 4825–4832
41. Clement, A. M., Nguyen, M. D., Roberts, E. A., Garcia, M. L., Boillee, S., Rule, M., McMahon, A. P., Doucette, W., Siwek, D., Ferrante, R. J., Brown, R. H., Jr., Julien, J. P., Goldstein, L. S., and Cleveland, D. W. (2003) *Science* 302, 113–117
42. Urushitani, M., Sik, A., Sakurai, T., Nukina, N., Takahashi, R., and Julien, J. P. (2006) *Nat. Neurosci.* 9, 108–118
43. Arrasate, M., Mitra, S., Schweitzer, E. S., Segal, M. R., and Finkbeiner, S. (2004) *Nature* 431, 805–810
44. Saudou, F., Finkbeiner, S., Devys, D., and Greenberg, M. E. (1998) *Cell* 95, 55–66
45. Schaffar, G., Breuer, P., Boteva, R., Behrends, C., Tzvetkov, N., Strippel, N., Sakahira, H., Siegers, K., Hayer-Hartl, M., and Hartl, F. U. (2004) *Mol. Cell.* 15, 95–105
46. Nucifora, F. C., Jr., Sasaki, M., Peters, M. F., Huang, H., Cooper, J. K., Yamada, M., Takahashi, H., Tsuji, S., Troncoso, J., Dawson, V. L., Dawson, T. M., and Ross, C. A. (2001) *Science* 291, 2423–2428

Exp. Anim. 55(1), 35–43, 2006

The Region-Specific Functions of Two Ubiquitin C-Terminal Hydrolase Isozymes along the Epididymis

Jungkee KWON[1, 3], Satoshi SEKIGUCHI[2], Yu-Lai WANG[1], Rieko SETSUIE[1], Yasuhiro YOSHIKAWA[2], and Keiji WADA[1]

[1]*Department of Degenerative Neurological Diseases, National Institute of Neuroscience, National Center of Neurology and Psychiatry, 4–1–1 Ogawahigashi, Kodaira, Tokyo 187-8502,*
[2]*Department of Biomedical Science, Graduate School of Agricultural and Life Sciences, The University of Tokyo, 1–1–1 Yayoi, Bunkyo-ku, Tokyo 113-8657, Japan, and*
[3]*Laboratory of Animal Medicine, College of Veterinary Medicine, Chonbuk National University, 664–14 Duckjin-Ku, Jeonju 561-756, Korea*

Abstract: *We previously showed that* gad *mice, which are deficient for ubiquitin C-terminal hydrolase L1 (UCH-L1), have a significantly increased number of defective spermatozoa, suggesting that UCH-L1 functions in sperm quality control during epididymal maturation. The epididymis is the site of spermatozoa maturation, transport and storage. Region-specific functions along the epididymis are essential for establishing the environment required for sperm maturation. We analyzed the region-specific expression of UCH-L1 and UCH-L3 along the epididymis, and also assessed the levels of ubiquitin, which has specificity for UCH-L1. In wild-type mice, western blot analysis demonstrated a high level of UCH-L1 expression in the caput epididymis, consistent with ubiquitin expression, whereas UCH-L3 expression was high in the cauda epididymis. We also investigated the function of UCH-L1 and UCH-L3 in epididymal apoptosis induced by efferent duct ligation. The caput epididymides of* gad *mice were resistant to apoptotic stress induced by efferent duct ligation, whereas* Uchl3 *knockout mice showed a marked increase in apoptotic cells following ligation. In conclusion, the response of* gad *and* Uchl3 *knockout mice to androgen withdrawal suggests a reciprocal function of the two UCH enzymes in the caput epididymis.*
Key words: *apoptosis, epididymis, ubiquitin, UCH*

Introduction

The mammalian epididymis is a highly convoluted tubule that connects the efferent ducts of the testis to the vas deferens [2, 8]. The epididymis is composed of three distinct compartments, caput (head), corpus (body) and cauda (tail), each having a specific role in sperm maturation, sustenance, transport, and storage [2, 6]. However, the molecular basis for the maturation process remains largely unknown.

It has been suggested that the epididymis acts as a quality control organ to eliminate defective spermato-

(Received 12 August 2005 / Accepted 4 November 2005)
Address corresponding: K. Wada, Department of Degenerative Neurological Diseases, National Institute of Neuroscience, National Center of Neurology and Psychiatry, 4–1–1 Ogawahigashi-cho, Kodaira, Tokyo 187-8502, Japan

zoa before ejaculation [37]. The epididymis is an organ with voluminous protein traffic between the epithelium and lumen. Numerous proteins, secreted in an apocrine manner by the epididymal epithelium, are implicated in spermatozoa maturation [18]. Two major components of the ubiquitin-dependent proteolytic pathway, ubiquitin and UCH-L1 (PGP9.5), are expressed in epididymal tissue [10, 35]. Ubiquitin is present in human seminal plasma [26], and defective spermatozoa become ubiquitinated during epididymal passage [23, 37]. Our previous work showed that UCH-L1 associates with monoubiquitin and stabilizes its expression [31]. In addition, it has been suggested that UCH-L1 functions as a regulator of apoptosis via the ubiquitin pathway [13, 23, 25]. We found that testes of gracile axonal dystrophy (*gad*) mice, which lack UCH-L1, have reduced ubiquitin levels and are resistant to cryptorchid injury–mediated germ cell apoptosis [25]. Furthermore, our recent work demonstrated that the percentage of morphologically abnormal spermatozoa is significantly higher in *gad* mice, compared with wild-type mice [23].

Two mouse UCH isozymes, UCH-L1 and UCH-L3, are strongly but reciprocally expressed in the testis during spermatogenesis [25], suggesting that these proteins have distinct functions in the testis [23], even though they have high amino acid sequence identity and share significant structural similarity [21]. The functional regionalization of the epididymis is delineated at the molecular level by regional differences in gene expression [16–19]. Regional differences along the epididymis might be essential characteristics of the environment required for sperm quality control. Although it has been shown that UCH-L1 and UCH-L3 have reciprocal functions with respect to cryptorchid injury, their molecular functions in regulating sperm quality during epididymal passage are not fully understood. Thus, we examined the epididymal expression of UCH-L1 and UCH-L3 with regard to their involvement in the regulation of apoptosis. In addition, we assessed the reciprocal functions of these two proteins in the epididymis.

Materials and Methods

Animals

We used *gad* (CBA/RFM) [34] and *Uchl3* knockout (C57BL/6J) [21] male mice at 10 weeks of age. The *gad* mouse is an autosomal recessive mutant that was obtained by crossing CBA and RFM mice. The *gad* line has been maintained by intercrossing for more than 20 generations [34]. *Uchl3* knockout mice were generated by the standard method [21] using homologously recombinant ES cells, and the knockout line has been back-crossed several times to C57BL/6J mice. Both strains are maintained at our institute. Animal care and handling were in accordance with our institutional regulations for animal care and were approved by the Animal Investigation Committee of the National Institute of Neuroscience, National Center of Neurology and Psychiatry.

Unilateral efferent duct ligation

Animals were either left intact to serve as controls or were unilaterally ligated at the efferent duct [9, 38]. Four mice in each group were anesthetized with pentobarbital (Abbott Laboratories, North Chicago, IL), and the testis and epididymis on the right side were exposed through a scrotal incision. The thin avascular attachment joining the initial segment of the epididymis to the tunica albuginea was cut to permit exposure of the efferent ducts coursing above and parallel to the vascular supply. A silk suture was passed by needle through the thin sheet of connective tissue between the ductules and the blood vessels, and the efferent ducts were occluded by ligation. Mice were sacrificed 2 or 4 days after ligation. Both epididymides were immersed in 4% paraformaldehyde for at least 24 hr before they were dehydrated and embedded in paraffin [22].

Histological and immunohistochemical assessment of the epididymis

The caput, corpus and cauda epididymides along the epididymal region embedded in paraffin were cut into 4-μm sections and stained with hematoxylin and eosin. Light microscopy was used for routine observations. For immunohistochemical staining, the sections were incubated with 10% goat serum for 1 h at room temperature followed by incubation overnight at 4°C with a rabbit polyclonal antibody raised against peptides within UCH-L1 or UCH-L3 (1:1,000 dilution; peptide antibodies [24]) and ubiquitin (1:500; DakoCytomation, Glostrup, Denmark) in PBS containing 1% BSA. Sections were then incubated for 1 h with biotin-conjugated anti-rabbit IgG diluted 1:200 in PBS, followed by

Vectorstain ABC-PO (Vector Laboratories, Burlingame, CA) for 30 min at room temperature. Sections were developed using 3,3'-diaminobenzidine and counterstained with hematoxylin.

In situ apoptosis was detected by TUNEL (TdT-mediated nick end-labeling) staining with the DeadEnd Fluorometric TUNEL system (Promega, Madison, WI) according to the manufacturer's instructions, to identify apoptotic cells in situ via specific labeling of nuclear DNA fragmentation. Quantification was performed using four mice on each of postoperative days 0, 2 and 4. The total number of apoptotic cells was determined by counting the positively stained nuclei in each caput epididymis section [9]. Four sections from each mouse and 100 total circular tubules per group were processed.

Western blotting

Western blots were performed as previously reported [24]. Total protein (10 μg/lane) from each epididymal region including spermatozoa was subjected to SDS-polyacrylamide gel electrophoresis using 15% gels (Perfect NT Gel, DRC, Japan). Proteins were electrophoretically transferred to polyvinylidene difluoride membranes (Bio-Rad, Hercules, CA) and blocked with 5% non-fat milk in TBS-T (50 mM Tris base, pH 7.5, 150 mM NaCl, 0.1% (w/v) Tween-20). The membranes were incubated individually with primary antibodies to monoubiquitin (1:1,000; u5379, Sigma-Aldrich, St. Louis, MO), UCH-L1 and UCH-L3 (1:1,000 dilution; anti-peptide antibodies [24]), p53, Bax, and Bcl-xL (1:1,000 dilution; all from Cell Signaling Technology, Beverly, MA), and Bcl-2 (1:500; Transduction Laboratories, Franklin Lakes, NJ). Blots were further incubated with peroxidase-conjugated goat anti-mouse IgG or goat anti-rabbit IgG (1:5,000 dilution; Pierce, Rockford, IL) for 1 h at room temperature. Immunoreactions were visualized using SuperSignal West Dura Extended Duration Substrate (Pierce) and analyzed using a ChemiImager (Alpha Innotech, San Leandro, CA). Each protein level was normalized to α-tubulin following analysis with a ChemiImager using AlphaEase software.

Statistical analysis

The mean and standard deviation were calculated for all data (presented as mean ± SD). Student's *t*-test was used for statistical analysis.

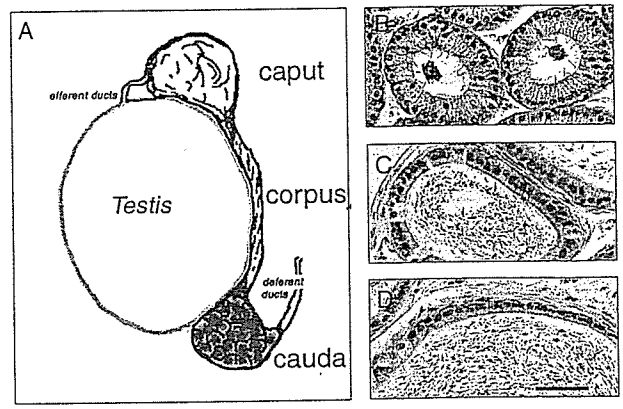

Fig. 1. A: Diagram of the epididymis. B–D: Morphology of the caput (B), corpus (C) and cauda (D) epididymidis from a wild-type mouse. Magnification, 200×. *Scale bar*, 40 μm.

Results

Levels of UCH-L1 and UCH-L3 in individual epididymal regions

The epididymis is a single long, coiled tubule situated on the surface of the testis (Fig. 1A). The epididymal epithelium is composed of four major cell types, principal cells, basal cells, clear cells and narrow cells [7], and can be divided anatomically and functionally into three regions, the caput, corpus and cauda epididymis (Fig. 1B, C, D). We used western blotting to characterize UCH-L1 and UCH-L3 levels along the epididymis (Fig. 2). In wild-type mice, the level of UCH-L1 was highest in the caput epididymis and that of UCH-L3 was highest in the cauda epididymis. UCH-L1 and UCH-L3 were not observed in *gad* and *Uchl3* knockout mice, respectively (Fig. 2; comparison of UCH-L1 and UCH-L3 levels with those in wild-type control mice).

Immunohistochemistry of UCH-L1, UCH-L3 and ubiquitin in the epididymis

Under light microscopy, granular and diffuse UCH-L1 and UCH-L3 immunoreactivity was detected in many epithelial cells of the caput, corpus and cauda epididymis in wild-type mice (Fig. 3A, C). Granular immunoreactivity to ubiquitin was seen in the epithelial cells of the epididymis (Fig. 3B). The distribution of ubiquitin in the corpus and cauda epididymal epithelial cells was similar to that of the caput epididymis,